

# Palaeogeography, Palaeoclimatology, Palaeoecology

## Climate variability during MIS 20-18 as recorded by alkenone-SST and calcareous plankton in the Ionian Basin (central Mediterranean)

--Manuscript Draft--

<b>Manuscript Number:</b>	PALAEO-D-20-00060
<b>Article Type:</b>	Research Paper
<b>Keywords:</b>	Lower-Middle Pleistocene, MIS 19, southern Italy, alkenone-SST, coccolithophores, planktonic foraminifera
<b>Corresponding Author:</b>	Maria Marino Dipartimento di Scienze della Terra e Geoambientali, University of Bari Bari, Bari Italy
<b>First Author:</b>	Maria Marino
<b>Order of Authors:</b>	Maria Marino Angela Girone, PhD Salvatore Gallicchio, PhD Timothy Herbert, Full Professor Marina Addante, Bachelor's degree Pietro Bazzicalupo, PhD Ornella Quivelli, PhD Franck Bassinot Adele Bertini, PhD Sebastien Nomade Neri Ciaranfi, Full Professor Patrizia Maiorano, PhD
<b>Manuscript Region of Origin:</b>	Europe
<b>Abstract:</b>	<p>This study shows the first Mediterranean high-resolution record of alkenone-derived sea surface temperature (SST) in the marine sediments outcropping at the Ideale section (IS) (southern Italy, central Mediterranean) from late marine isotope stage (MIS) 20 - through early MIS 18 interval. The SST pattern evidences glacial-interglacial up to centennial-scale temperature variation, with lower values (~13°C) in late MIS 20 and substage 19b, and higher values (up to 21°C) in MIS 19c and MIS 19a interstadials. The SST data are combined with the new calcareous plankton analysis and the available, chronologically well-constrained carbon and oxygen isotope records in the IS. The multi-proxy approach, location of the IS near the Italian coasts, its lower circalittoral-upper bathyal depositional setting, and high sedimentation rate allow to document long- and short-term paleoenvironmental modifications (sea level, rainfall, inorganic/organic/fresh water input to the basin), as a response to regional and global climate changes. The combined proxies reveal the occurrence of a terminal stadial in late MIS 20 (here Med-H TIX ), and warm-cold episodes (here Med-BA TIX and Med-YD TIX ) during Termination IX (TIX), which recall those that occurred through the last termination (TI). During these periods and the following sapropelic layer (insolation cycle 74, 784 ka) in the early MIS 19, higher frequency internal changes are synchronously recorded by all proxies. The substage MIS 19c is warm but quite unstable, with several episodes of paleoenvironmental changes, associated with fluctuating tropical-subtropical water inflow through the Gibraltar Strait, variations of the cyclonic regime in the Ionian basin, and the southward shift of westerly winds and winter precipitation over southern Europe and Mediterranean basin. Three high-amplitude millennial-scale oscillations in the patterns of SST and calcareous plankton key species during MIS 19a are interpreted as linked to global changes in temperature as well as in salinity and in periodical column water stratification and mixing.</p>

	<p>The main processes involved in the climate variability included changes in oceanographic exchanges through the Gibraltar Strait during modulations of Atlantic meridional overturning circulation and/or variations in atmospheric dynamics related to the influence of westerly and polar winds acting in the paleo-Ionian basin. A strong climate teleconnection between the North Atlantic and Mediterranean has been documented, and a prominent role of atmospheric processes in the central Mediterranean has been evidenced by comparing data sets at the IS with Italian and extra-Mediterranean marine and terrestrial records.</p>
<p><b>Suggested Reviewers:</b></p>	<p>Antonio Caruso, PhD  Full Professor, Università degli Studi di Palermo Dipartimento di Scienze della Terra e del Mare  antonio.caruso@unipa.it  specialist of planktonic foraminifera</p> <hr/> <p>José Abel Flores, PhD  Full Professor, Universidad de Salamanca  flores@usal.es  specialist of coccolithophores, paleoclimate, paleoceanography</p> <hr/> <p>Martin Head  Full Professor, Brock University  mjhead@brocku.ca  specialist of Pleistocene climatostratigraphy</p> <hr/> <p>Maria Triantaphyllou, PhD  mtriant@geol.uao.gr  specialist of Mediterranean coccolithophores paleoecology</p> <hr/> <p>Barbara Balestra, PhD  balestra@american.edu  specialist of coccolithophore</p>

Dear Editor,

I would like to submit for publication the manuscript

*Climate variability during MIS 20-18 as recorded by alkenone-SST and calcareous plankton in the Ionian Basin (central Mediterranean),*

by the authors Maria Marino (corresponding author), Angela Girone, Salvatore Gallicchio, Timothy Herbert, Marina Addante , Pietro Bazzicalupo, Ornella Quivelli, Franck Bassinot, Adele Bertini, Sebastien Nomade, Neri Ciaranfi, Patrizia Maiorano.

All the co-authors agree with this submission.

Best Regards

Maria Marino  
and co-authors

The first Mediterranean alkenone-based SST pattern is presented through MIS20-MIS18

The SST data are compared with new high-resolution calcareous plankton variations

The records show orbital-suborbital up to centennial-scale climate changes

Strong similarity occurs in the climate oscillations between Terminations IX and I

Oceanographic and atmospheric mechanisms drive paleoenvironmental changes

1 **Climate variability during MIS 20-18 as recorded by alkenone-SST and calcareous plankton**  
2 **in the Ionian Basin (central Mediterranean)**

3  
4 Maria Marino<sup>1\*</sup>, Angela Girone<sup>1</sup>, Salvatore Gallicchio<sup>1</sup>, Timothy Herbert<sup>2</sup>, Marina Addante<sup>1</sup>, Pietro  
5 Bazzicalupo<sup>1</sup>, Ornella Quivelli<sup>1</sup>, Franck Bassinot<sup>3</sup>, Adele Bertini<sup>4</sup>, Sebastien Nomade<sup>3</sup>, Neri  
6 Ciaranfi<sup>1</sup>, Patrizia Maiorano<sup>1</sup>

7  
8 1\*: Dipartimento di Scienze della Terra e Geoambientali, University of Bari, Italy, [maria.marino@uniba.it](mailto:maria.marino@uniba.it)

9 2: Brown University, Providence, RI, United States

10 3: Laboratoire des Sciences du Climat et de L'Environnement, UMR8212, LSCE/IPSL, CEA-CNRS-UVSQ and  
11 Université Paris-Saclay, Gif-Sur-Yvette, France

12 4: Dipartimento di Scienze della Terra, University of Florence, Italy

13  
14  
15  
16 **Abstract**

17 This study shows the first Mediterranean high-resolution record of alkenone-derived sea surface  
18 temperature (SST) in the marine sediments outcropping at the Ideale section (IS) (southern Italy,  
19 central Mediterranean) from late marine isotope stage (MIS) 20 - through early MIS 18 interval.  
20 The SST pattern evidences glacial-interglacial up to centennial-scale temperature variation, with  
21 lower values (~13°C) in late MIS 20 and substage 19b, and higher values (up to 21°C) in MIS 19c  
22 and MIS 19a interstadials. The SST data are combined with the new calcareous plankton analysis  
23 and the available, chronologically well-constrained carbon and oxygen isotope records in the IS.  
24 The multi-proxy approach, location of the IS near the Italian coasts, its lower circalittoral-upper  
25 bathyal depositional setting, and high sedimentation rate allow to document long- and short-term  
26 paleoenvironmental modifications (sea level, rainfall, inorganic/organic/fresh water input to the  
27 basin), as a response to regional and global climate changes. The combined proxies reveal the  
28 occurrence of a terminal stadial in late MIS 20 (here Med-H<sub>TIX</sub>), and warm-cold episodes (here  
29 Med-BA<sub>TIX</sub> and Med-YD<sub>TIX</sub>) during Termination IX (TIX), which recall those that occurred  
30 through the last termination (TI). During these periods and the following sapropelic layer  
31 (insolation cycle 74, 784 ka) in the early MIS 19, higher frequency internal changes are

32 synchronously recorded by all proxies. The substage MIS 19c is warm but quite unstable, with  
33 several episodes of paleoenvironmental changes, associated with fluctuating tropical-subtropical  
34 water inflow through the Gibraltar Strait, variations of the cyclonic regime in the Ionian basin, and  
35 the southward shift of westerly winds and winter precipitation over southern Europe and  
36 Mediterranean basin. Three high-amplitude millennial-scale oscillations in the patterns of SST and  
37 calcareous plankton key taxa during MIS 19a are interpreted as linked to global changes in  
38 temperature as well as in salinity and in periodical column water stratification and mixing.  
39 The main processes involved in the climate variability include changes in oceanographic exchanges  
40 through the Gibraltar Strait during modulations of Atlantic meridional overturning circulation  
41 and/or variations in atmospheric dynamics related to the influence of westerly and polar winds  
42 acting in the paleo-Ionian basin. A strong climate teleconnection between the North Atlantic and  
43 Mediterranean is discussed, and a prominent role of atmospheric processes in the central  
44 Mediterranean is evidenced by comparing data sets at the IS with Italian and extra-Mediterranean  
45 marine and terrestrial records

46

47 **Keywords:** Lower-Middle Pleistocene, MIS 19, southern Italy, marine biomarkers, coccolithophores, planktonic  
48 foraminifera

49

## 50 **1. Introduction**

51 Marine Isotope Stage (MIS) 19 stage is generally considered an excellent analogue for the  
52 current interglacial, due to the same astronomical configuration of orbital parameters: low  
53 eccentricity and an obliquity maximum almost in phase with the northern Hemisphere precession  
54 minimum. For this reason, any high-resolution study of MIS 19 can bring invaluable pieces of  
55 information about the natural duration of the current interglacial and the inception of next glacial in  
56 absence of human impact. MIS 19 is characterized by an orbital/suborbital climate variability that is  
57 evidenced by the partition in substages a, b, and c in the  $\delta^{18}\text{O}$  oscillations (Railsback et al., 2015),

58 associated to 19.3, 19.2, and 19.1 events (Bassinot et al., 1994). They may have relevant  
59 implications in climatostratigraphy (Miller and Wright, 2017), coherently with the wide use of  
60 oxygen isotope signature for Quaternary chronostratigraphic subdivision. Specifically, the Lower-  
61 Middle Pleistocene chronostratigraphic boundary, close to the Matuyama-Brunhes paleomagnetic  
62 reversal, is associated worldwide to the MIS 19c/MIS 19b transition at ~773 ka (Head, 2019, and  
63 reference therein). Millennial-scale variations have been also highlighted within MIS 19 as a result  
64 of local and North Hemisphere oceanic-atmosphere dynamics. A distinct occurrence of the first  
65 climate deterioration marked by MIS 19b after the full interglacial, and climate oscillations in MIS  
66 19a, have been revealed by recent high-resolution proxies in several marine (Kleiven et al., 2011;  
67 Tzedakis et al., 2012; Emanuele et al., 2015; Ferretti et al., 2015; Sánchez Goñi et al., 2016;  
68 Nomade et al., 2019) and lacustrine sediments (Giaccio et al., 2015; Regattieri et al., 2019), and ice  
69 core (e.g. Pol et al., 2010).

70 These climate episodes, occurring at a wide scale (Nomade et al., 2019), may have not been  
71 given coherent chronologies, possibly due to different age-model strategies and the fact that  
72 different proxies may have been used to identify them. This makes it difficult to correlate climate  
73 stages and events with accuracy and to interpret climate dynamics and temporal relationship (ie.  
74 lead/lag) between high and mid latitudes or between marine and terrestrial realms, thus preventing  
75 the comprehension of cause-effect connections and the climate propagation of changes at regional  
76 and global scale.

77 The on land marine Ideale section (IS), as part of the Montalbano Jonico section (MJS, southern  
78 Italy) crossing MIS 37-MIS 16, offers the opportunity to improve the paleoclimate framework of  
79 MIS 19 due to its high sedimentation rate and environmental setting. It was deposited in lower  
80 circalittoral-upper bathyal, not far from a peninsular coastline, and thus registered even slight  
81 climatically induced modifications such as changes in sea level, precipitation, and inorganic/organic  
82 input from land. The water depth of the sediments is also suitable to provide numerous marine

83 proxy data, in the form of planktonic and benthic foraminifera, coccolithophores, and marine  
84 biomarkers. The IS has been extensively studied in recent years due to its potential to represent the  
85 Lower-Middle Pleistocene chronostratigraphic boundary (e.g. Ciaranfi et al., 2010; Maiorano et al.,  
86 2010, 2016a; Bertini et al., 2015; Marino et al., 2015, 2016; Petrosino et al., 2015; Simon et al.,  
87 2017; Nomade et al., 2019). Short-term climate episodes in the latest MIS 20 and Termination IX  
88 (TIX) have been referred to Heinrich-like (Ht), Bølling-Allerød-like (BA<sub>t</sub>), and Younger-Dryas like  
89 (YD<sub>t</sub>) based on multi-proxy investigation thus suggesting a climate variability comparable to that  
90 documented during the last deglaciation (Maiorano et al., 2016a). The latter authors suggested the  
91 need of higher resolution data set to support these evidences in a finer constrained time frame. The  
92 more recent, very high-resolution benthic (*Cassidulina carinata*, *Melonis barleeanum*)  $\delta^{18}\text{O}$  and  
93  $\delta^{13}\text{C}$  records (Nomade et al., 2019) have improved the chronology of the IS, detailing the pattern of  
94 MIS 19 substages and the three interstadial phases in MIS 19a (19a-1, 19a-2, and 19a-3),  
95 highlighting the centennial-scale timing of these climate oscillations and their worldwide  
96 correlability.

97 In the present work we present new high-resolution alkenone-SST data acquired at the IS, which  
98 are the first recorded in the Mediterranean Sea for the time interval spanning MIS 20-MIS 18 and  
99 may improve the understanding of the climate evolution as recorded in marine environment. New  
100 quantitative calcareous plankton (coccolithophores and foraminifera) results, obtained on the same  
101 samples used for marine biomarkers and for the isotopic study of Nomade et al. (2019), are also  
102 presented, providing a paleoecological window into synchronous marine response to major  
103 environmental modifications. The combination of this new data set with the detailed benthic isotope  
104 records available at the IS provides useful insights into i) the marine surface/subsurface water  
105 conditions in the central Mediterranean during an important interglacial of mid-Pleistocene  
106 transition considered the best analogue of the current interglacial (Holocene), ii) the terminal stadial  
107 event in late MIS 20 and its oceanographic-atmospheric connection with North Atlantic climate,



108 iii) the high frequency climate variability across TIX, making it possible to better address its  
109 apparent similarity with the rapid variability that occurred during TI. The comparison of new data  
110 with selected high-resolution climate references from North Atlantic Ocean provides additional  
111 highlights on central Mediterranean response to local or global climate via atmospheric-  
112 oceanographic processes.

113

## 114 **2. Oceanography**

115 Sediments of the MJS were deposited in the paleo Gulf of Taranto (Fig. 1D), in the north Ionian  
116 Sea. At this location important detrital sediment supply derives mainly from Apennines rivers  
117 (Goudeau et al., 2013). Sediments from the Po River and other Apennines rivers may also arrive in  
118 the eastern Gulf of Taranto through the Western Adriatic Current (WAC) (Fig. 1D). This low  
119 salinity (37.2 PSU along the southern Italian coast) nutrient-rich current flows southward in a  
120 narrow coastal band from the northern Adriatic Sea, and mixes with the more saline Ionian waters  
121 (up to 39.5 PSU in the central Ionian Sea) (Poulain, 2001; Bignami et al., 2007; Turchetto et al.,  
122 2007; Grauel and Bernasconi, 2010). The WAC has higher influence in winter and spring (Poulain,  
123 2001) than in summer and is characterized by significant inter-annual variability (Milligan and  
124 Cattaneo, 2007). In the Gulf of Taranto the highly saline Levantine Intermediate Water (LIW),  
125 flowing from the central Ionian Sea, may be recorded at the water depth of 200-600 m (Savini and  
126 Corselli, 2010). The Northern Ionian Gyre (NIG) that has decadal scale cyclonic and anticyclonic  
127 phases (Civitarese et al., 2010) characterizes the central open ocean area of the Gulf of Taranto. The  
128 cyclonic phase is characterized by saltier Levantine/Cretan Intermediate Waters (LIW/CIW) that  
129 flow northward into the Adriatic, while anticyclonic phase records advection of less saline Ionian  
130 water diluted by Modified Atlantic Waters (MAW) (Civitarese et al., 2010). In the first case poor-  
131 nutrient LIW/CIW waters enter the north Ionian Sea and south Adriatic Sea, while the influx of  
132 MAW during anticyclonic phase favours upwelling events and nutrients supply at the periphery of

133 the anticyclonic NIG along the souther Italian coasts before reaches the south Adriatic Sea  
134 (Civitarese et al., 2010). The alternating anticyclonic and cyclonic states are known as Adriatic-  
135 Ionian bimodal oscillation system (Civitarese et al., 2010; Gačić et al., 2010) that may influence  
136 nutrient distribution and phytoplankton growth (Civitarese et al., 2010, Batistić et al., 2017).

137 Modern annual mean SSTs in the Gulf of Taranto are about 19.7 °C (Pujol and Vergnaud-  
138 Grazzini, 1995). During summer, they vary from 26°C to 15°C at the surface and at 50 m depth,  
139 respectively, and the water column is stratified (Zonneveld et al., 2008; Grauel and Bernasconi,  
140 2010). During winter, SSTs vary between 13°C and 15°C. These seasonal temperature changes can  
141 influence the upper 100 m of the water column (Socal et al., 1999; Locarnini et al., 2010).

142 Today, the high latitude North Atlantic and Arctic climate perturbations rapidly spread to the  
143 northern hinterlands of the Mediterranean and are channelized in mountain valleys through intense  
144 northerly flows of cold and dry air masses ('Mistral', 'Bora', 'Vardar' winds) over the northwestern  
145 Mediterranean, the Adriatic and the Aegean basins (Mariolopoulos, 1961; Leaman and Scott, 1991;  
146 Poulos et al., 1997). These polar and continental winter airflows cause intense evaporation and  
147 cooling of the sea surface and terrestrial vegetation (e.g., Leaman and Schott, 1991; Saaroni et al.,  
148 1996; Poulos et al., 1997; Maheras et al., 1999; Casford et al., 2003; Rohling et al., 2009).

149

### 150 **3. Geological setting and stratigraphy**

151 The IS, as part of the Montalbano Jonico succession (MJS), crops out in the south-western  
152 margin of the Bradanic Trough, at about 16 km inland from the Ionian Coast (40°17'29.52" N  
153 16°33'10.58"E) (Fig. 1). The Bradanic Trough (e.g. Casnedi, 1988), located between the Apennines  
154 Chain to the west and the Apulian foreland eastward (Fig. 1B), is a foredeep basin of the post-  
155 Messinian Apennines. Its origin and evolution are associated with the eastward roll-back of the  
156 subduction hinge of the Apulia platform and the evolution of the external Apennines thrust front  
157 during the Plio-Pleistocene (e.g., Patacca and Scandone, 2007 and references therein). The foredeep

158 was characterized by high rates of subsidence until the Calabrian, after which it underwent a  
159 diachronous uplift starting from the Genzano-Banzi area during late Calabrian and proceeding  
160 southeastward to the actual Ionian coast by Holocene time. In the late Calabrian, the central sector  
161 of the Bradanic Trough emerged while the southern sector, where the study section is located, was  
162 still subsiding. The central foredeep sector reached its maximum deepening in the Early-Middle  
163 Pleistocene (e.g., Maiorano et al., 2016a). From the Middle Pleistocene, the sedimentation reveals a  
164 shoaling-upward trend due to the uplift of the area (uplift rate of 0.1–0.5 mm/years, e.g. Doglioni et  
165 al., 1996) that led to the emersion of the area since 0.6/0.7 Ma. Regionally, the gradual emersion of  
166 the area is testified by several continental and marine terraces, represented by transitional and  
167 continental deposits of ancient alluvial and costal plains developed between 0.7 Ma and the Late  
168 Pleistocene (e.g. Vezzani, 1967; Brückner H., 1980 a, b; Pescatore et al., 2009; Sauer et al., 2010,  
169 Boenzi et al., 2014).

170 The MJS (Fig. 1C) belongs to the argille subapennine informal unit (Azzaroli et al., 1968),  
171 representing its middle-upper portion, Early to Middle Pleistocene in age (Ciaranfi et al., 2010). It  
172 consists of coarsening-upwards deposits ranging from silty clays to silty sands and includes nine  
173 tephra layers (V1–V9) (Fig. 1C). The tephra layers (V1–V9) were chemically and mineralogically  
174 characterized and correlated to analogous layers from south-central Italy lacustrine and marine  
175 successions, within a Lower-Middle Pleistocene Mediterranean tephrostratigraphic frame (Petrosino  
176 et al., 2015). The MJS, in its lower part, includes five dark horizons interpreted as sapropel layers  
177 (D'Alessandro et al., 2003; Stefanelli, 2004; Stefanelli et al., 2005; Maiorano et al., 2008) and  
178 correlated, from oldest to youngest, to insolation cycles i-112, i-104, i-102, i-90, and i-86, based on  
179 the Mediterranean sapropel stratigraphy of Lourens (2004) and Lourens et al. (2004). The  
180 calcareous nannofossil biostratigraphy indicates that the entire succession belongs to the small  
181 *Gephyrocapsa* and *Pseudoemiliana lacunosa* zones, based on the biostratigraphic scheme of Rio et  
182 al. (1990) (Fig. 1C). Several deepening-shallowing cycles, from bathyal to circalittoral

183 environments, have been recognized based on micro- and macro-invertebrate benthic assemblages  
184 (D'Alessandro et al., 2003; Stefanelli, 2003; Ciaranfi and D'Alessandro, 2005; Girone, 2005).  
185 Specifically, benthic paleocommunities from the lower part of succession (Interval A) indicated  
186 upper slope environments, with a maximum depth of ca. 500 m, while paleocommunities of upper  
187 portion (Interval B) pointed out to outer to inner shelf settings with short-term deepening towards  
188 upper slope.

189 The IS, in Interval B, consists of clays and silty clays bracketed by two tephra layers, V3 and V4.  
190 The V3 and V4 layers were radiometrically dated and their  $^{40}\text{Ar}/^{39}\text{Ar}$  ages are  $801.2 \pm 19.5$  ka  
191 (Maiorano et al., 2010),  $773.9 \pm 1.3$  ka (Petrosino et al., 2015), respectively. The V3 tephra is  
192 located within the MIS 20 interval (at 820 cm) and V4 is at the transition from MIS 19c to MIS 19b  
193 (at 3660 cm) (Fig. 1C). Due to its high stratigraphic value in constraining the MIS 19c/19b  
194 transition, coincident with the  $^{10}\text{Be}/^9\text{Be}$  peak interpreted as the Earth magnetic field collapse during  
195 the Matuyama-Brunhes reversal (Simon et al., 2017), V4 has been re-dated at the LSCE laboratory  
196 (France). New dating provided a  $^{40}\text{Ar}/^{39}\text{Ar}$  age of  $774.1 \pm 0.9$  ka (Nomade et al., 2019), which is in  
197 good agreement with the Ar/Ar age estimate of Petrosino et al. (2015). The dark grey bands (Fig.  
198 1C) correspond to higher kaolinite and smectite content and increased chemical weathering on land  
199 (Maiorano et al., 2016a); the clay fraction increases significantly (20–31%, average 24%) from the  
200 onset of MIS 19 upwards, although several fluctuations have been observed through the interval  
201 encompassing MIS 19a towards MIS 18. In contrast, the light grey bands are related to increases of  
202 quartz and dolomite associated with enhanced supplies of the coarser detrital mineral components  
203 into the basin (Maiorano et al., 2016a). Dark and light intervals correspond to lower (interglacial,  
204 interstadials) and higher (glacial, stadials) benthic  $\delta^{18}\text{O}$  values, respectively, suggesting the glacio-  
205 eustatic/climate control on sedimentary features of the IS. However, the influx of fresh water of on  
206 land origin during wetter climate was not excluded during lighter  $\delta^{18}\text{O}$  and darker sedimentation  
207 phases, in contrast to more arid climate during heavier  $\delta^{18}\text{O}$  intervals (Bertini et al., 2015; Nomade

208 et al., 2019). The shallowing-deepening cycles through MIS 20-18 are also highlighted by marine  
209 micro- and macrobenthic assemblages (D'Alessandro et al., 2003; Stefanelli, 2003; Aiello et al.,  
210 2015), and pollen distality index (Bertini et al., 2015). In detail, paleodepths range from about 100  
211 m to 180-200 m (Aiello et al., 2015) which implies a water column mainly distributed in the photic  
212 zone. A maximum flooding in the mid MIS 19c (MF, Fig. 1C) followed by the maximum depth  
213 interval (MD, Fig. 1C) are documented by D'Alessandro et al. (2003) based on the benthic macro-  
214 invertebrate communities.

215

## 216 **4. Methods**

217 Alkenones and calcareous plankton assemblages were investigated in 170 and 167 samples,  
218 respectively, from the same levels analyzed for the high-resolution isotope curves of Nomade et al.  
219 (2019). The sample spacing is between 20 and 40 cm and corresponds to a temporal resolution of  
220 200 years in MIS 20, down to about 100 years during selected intervals (mainly Termination IX and  
221 MIS 19a), according to the age-model of Nomade et al. (2019).

222

### 223 *4.1 Biomarker analyses*

224 Lipid biomarker extractions were carried out on 5g freeze-dried, ground samples by accelerated  
225 solvent extraction (Dionex ASE-200) at Brown University. The complexity of interfering peaks in  
226 the region where C<sub>37</sub> and C<sub>38</sub> alkenones elute via gas chromatography (GC), organic extracts were  
227 purified by silica gel flash column chromatography prior to GC analysis. Gas chromatography was  
228 carried out on an Agilent (60 m, DB-1 column) with the following parameters: GC performance  
229 was monitored by running a lab standard extract at the beginning and end of each run, and running  
230 replicates (“bookends”) of IS extracts within the run to rule out chromatographic drift. In addition to  
231 the U<sup>k</sup><sub>37</sub> index, we determined comparable C<sub>38</sub> unsaturation indices for quality control; the signal  
232 noise of these determinations was less than for the U<sup>k</sup><sub>37</sub> index, but they served a redundancy checks

233 that would have indicated the presence of outliers possibly indicating compounds interfering with  
234 alkenones in GC analysis. Reproducibility was  $\sim 0.01 U_{37}^k$  units and  $\sim 5\%$  relative error for  
235 C37total. Estimates of alkenone paleotemperature follow calibration of Müller et al. (1998).

236

#### 237 4.2 Microfossils

238 Analyses for planktonic foraminifera were carried out on the residue  $>150\ \mu\text{m}$  after the sediment  
239 was dried and washed on a  $63\ \mu\text{m}$  sieve. The residues were split until a representative aliquot,  
240 containing about 300 specimens, has been obtained. The species abundances were quantified as  
241 percentages on the total number of planktonic foraminifers. Sixteen species or species groups were  
242 distinguished: *Globigerinoides ruber* includes morphotype *Globigerinoides ruber* white, and  
243 *Globigerinoides elongatus* (sensu Aurahs et al., 2011); *Trilobatus sacculifer* includes *Trilobatus*  
244 *trilobus*, *Trilobatus sacculifer* and *Trilobatus quadrilobatus* (sensu Hemleben et al., 1989; André et  
245 al., 2013; Spezzaferrri et al., 2015). The SPRUDTS group (sensu Rohling et al., 1993)  
246 (*Globigerinella siphonifera*, *Hastigerina pelagica*, *Globoturborotalita rubescens*, *Orbulina*  
247 *universa*, *Beella digitata*, *Globoturborotalita tenella*, and *T. sacculifer*) and *G. ruber* were grouped  
248 as warm water indicators (foram-wwt). The criteria adopted for the taxonomy of *Neogloboquadrina*  
249 spp. are from Darling et al. (2006): *Neogloboquadrina incompta* corresponds to neogroboquadrinids  
250 previously referred to *N. pachyderma* (dextral) and includes intergrades between *N. pachyderma*  
251 (dextral) and *N. dutertrei*; *N. pachyderma* includes the left coiling specimens. It is a polar-subpolar  
252 taxon in the Northern Hemisphere (Bé and Tolderlund, 1971; Hemleben et al., 1989; Johannessen et  
253 al., 1994; Simstich et al., 2003; Darling et al., 2006) and has been found rare ( $< 5\%$ ) in central and  
254 eastern Mediterranean Sea during Pleistocene (e.g. Thunell, 1978; Rohling and Gieskes, 1989;  
255 Rohling et al., 1993; Hayes et al., 1999, 2005; Sprovieri et al., 2003, 2012; Triantaphyllou et al.,  
256 2009; Siani et al., 2010). Increases in the abundance of *N. pachyderma* has been used as a proxy of  
257 Atlantic cold (melt) water influx into Mediterranean (Hemleben et al., 1989; Pérez-Folgado et al.,

258 2003; Sierro et al., 2005; Girone et al., 2013; Capotondi et al., 2016; Marino et al., 2018). *N.*  
259 *incompta* is a cold and eutrophic taxon, indicative of deep chlorophyll maximum at the base of the  
260 euphotic layer (Hemleben et al., 1989; Reynolds and Thunnel., 1989; Pujol and Vergnaud-Grazzini,  
261 1995; Rohling et al., 1995). *G. bulloides*, due to its opportunistic behavior, has been used as an  
262 indicator of high nutrient content, the species preferring eutrophic condition related to upwelling,  
263 strong seasonal mixing or river input (Tolderlund and Bé, 1971; Hemleben et al., 1989; Pujol and  
264 Vergnaud Grazzini, 1995; Rohling et al., 1997; Bàrcena et al., 2004; Geraga et al., 2005, 2008). *G.*  
265 *inflata* has been used a proxy of cool-temperate waters, deep pycnocline, and ventilated conditions  
266 (Hemleben et al., 1989; Pujol and Vergnaud-Grazzini, 1995; Rohling et al., 1995; Barcena et al.,  
267 2004).

268 Slides for coccolithophore analysis were prepared according to Flores and Sierro (1997) to  
269 estimate absolute coccolith abundances. Quantitative analyses were performed using a polarized  
270 light microscope at 1000× magnification and abundances were determined by counting at least 500  
271 coccoliths of all sizes, in a varying number of fields of view. Species abundances were expressed as  
272 percentage and as N (coccolith/gram of sediment). The warm-water taxa *Umbilicosphaera sibogae*  
273 s.l., *Calciosolenia* spp., *Discosphaera tubifera*, *Rhabdosphaera clavigera*, *Umbellosphaera* spp.,  
274 *Oolithotus* spp., *Helicosphaera pavementum* were grouped together (nanno-wwt) according to their  
275 ecological preferences and their higher abundances during warmer and oligotrophic conditions  
276 (McIntyre and Bé, 1967; Winter et al., 1994; Ziveri et al., 2004; Baumann et al., 2004; Boeckel and  
277 Baumann, 2004; Saavedra-Pellitero et al., 2010; Palumbo et al., 2013; Maiorano et al., 2015;  
278 Marino et al., 2018). *Coccolithus pelagicus* ssp. *pelagicus*, a subarctic taxon (Baumann et al., 2000;  
279 Geisen et al., 2002), was used as an indicator of cold meltwater influx in mid-latitude North  
280 Atlantic Ocean (Parente et al., 2004; Marino et al., 2011, 2014; Amore et al., 2012; Maiorano et al.,  
281 2015), even in Mediterranean basin (Girone et al., 2013; Maiorano et al., 2016a; Marino et al.,  
282 2018; Trotta et al., 2019). Increases of *Florisphaera profunda* that thrive in the lower photic zone

283 were considered indicative of deep nutricline (Molfino and McIntyre, 1990). The taxon may also  
284 inhabit surface water when turbidity and low light occur due to too high surface detrital input and  
285 low light intensity (Ahagon et al., 1993; Colmenero-Hidalgo et al., 2004; Maiorano et al., 2008,  
286 2016a; Girone et al., 2013). Taxonomy of geophyrocapsids follows the criteria of Maiorano et al.  
287 (2013). *Helicosphaera carteri* has been used as a proxy of enhanced detrital input, surface water  
288 turbidity and low salinity (Colmenero-Hidalgo et al., 2004), conditions associated to higher runoff  
289 and enhanced nutrients (Bonomo et al., 2018) or cold glacial phases and low sea level in  
290 Mediterranean Sea (Weaver and Pujol, 1988; Colmenero-Hidalgo et al., 2004; Maiorano et al.,  
291 2013, 2015, 2016b; Marino et al., 2018).

292

## 293 **5. Results**

294 At the IS, SST pattern records values between 12 and  $\sim 22^{\circ}\text{C}$  (Fig. 2D). The lower SSTs  
295 characterizes the lower part of the studied section (MIS 20), substage MIS 19b and the stadial  
296 episodes in MIS 19a. On the other hand, higher temperatures are recorded in MIS 19c and  
297 interstadials 19a-1, 19a-2, and 19a-3 (Fig. 2D). Calcareous plankton key taxa used here for  
298 paleoenvironmental reconstruction show relevant fluctuations through time. Total coccoliths (tot N,  
299 Fig. 2F) have abundance mainly lower than 20 coccoliths/g ( $\times 10^7$ ) in MIS 20 and during TIX, and  
300 lower than 30 coccoliths/g ( $\times 10^7$ ) from MIS 19b towards the end of the studied section, with  
301 slightly increases up to 40 coccoliths/g ( $\times 10^7$ ) during interstadials in MIS 19a. Total N has higher  
302 values, up to 100 coccoliths/g ( $\times 10^7$ ), during MIS 19c. Coccolithophore wwt (nanno wwt, Fig.  
303 2G), although low in abundance throughout the section, has fluctuating increases in MIS 19c and  
304 interstadial 19a-2, with abundance never higher than 0.5 coccoliths/g ( $\times 10^7$ ). *F. profunda*  
305 generally has abundance lower than 1 coccoliths/g ( $\times 10^7$ ) while it shows major fluctuating  
306 increase up to 3.2 coccoliths/g ( $\times 10^7$ ) in MIS 19c (Fig. 3D). *Syracosphaera* spp. are a minor  
307 component of coccolithophore assemblage (Fig. 3F), however they records a distinct abundance



308 peak of 0.5 coccoliths/g ( $\times 10^7$ ) in the lower MIS 19c. The percentage abundances of planktonic  
309 foraminifera wwt (Fig. 2H) vary between 5 and 80% and depict glacial-interglacial and stadial-  
310 interstadial episodes with a few short-term minor increases during TIX. In particular, the relative  
311 abundances of *T. trilobatus* reach 3.5% in MIS 19c and MIS 19a-2 interstadial (Fig. 2H); *G. ruber*  
312 is a significant component reaching relative abundances up to 72% mainly starting from MIS 19c  
313 upwards (Fig. 3G). The polar-subpolar *C. pelagicus* ssp. *pelagicus* and *N. pachyderma* are more  
314 abundant, with values up to 22% and 5%, respectively, in MIS 20, during TIX and in MIS 19b as  
315 well as in colder phases of MIS 19a (Fig. 2 K-L). *H. carteri* shows a comparable pattern (Fig. 2M)  
316 with fluctuating relative abundances lower than 7.5%. *N. incompta* has discontinuous relative  
317 abundance, with peaks up to 17% in MIS 20 and TIX, in lower MIS 19c, and in short-term intervals  
318 of MIS 19a, while it is absent in the upper MIS 19c (Fig. 2I). *G. bulloides* is continuously present  
319 throughout the IS and shows variable abundances, which seem to increase in the upper portion of IS  
320 (Fig. 2J). *G. inflata* records higher abundances, up to 80%, in distinct periods of TIX and in the  
321 stadials of MIS 19a, whereas it is absent in MIS 19c and interstadial phases (Fig. 2N). *O. universa*  
322 shows abundance variations during the investigated interval, with more prominent peaks, up to 27%,  
323 in selected short-term intervals of TIX and in MIS 19a interstadials.

324

## 325 **6. Discussion**

326 Results are discussed starting from the lower portion of the studied record upwards focusing on  
327 environmental changes occurred in late MIS 20 and TIX (Fig. 2) to MIS 19 onset (Figs 2-3), and  
328 towards MIS 19b-19a, and MIS 18 beginning (Fig. 2). Comparisons with climate proxies from other  
329 extra-Mediterranean reference sections are presented in figure 4.

330

331 *6.1 Environmental changes through late MIS 20: the terminal stadial event Med-H<sub>TIX</sub>*

332 The lower part of the studied section (800-794 ka) is characterized by fluctuating values of SST  
333 between ~ 16 and 20°C (Fig. 2D). Upward, between 794 and 788.5 ka, a terminal stadial (sensu  
334 Hodell et al., 2015), hereafter named Med-H<sub>TIX</sub>, may be recognized, primarily based on the SST  
335 decreases and the polar-subpolar *N. pachyderma* and *C. pelagicus* ssp. *pelagicus* increase (Fig. 2 K-  
336 L). In more details, SSTs were at least 4-5°C cooler than pre-Med-H<sub>TIX</sub> (17-21°C) with fluctuating  
337 values mainly below 16°C, and minimum at 13°C. These values are compatible with  $\Delta^{47}$ -derived  
338 subsurface temperature of 12.1°C measured on benthic foraminifera at 794 ka (Peral et al., 2020).  
339 *C. pelagicus* ssp. *pelagicus* and *N. pachyderma* increase from percentages mainly below 3% and  
340 10%, to values up to 5% and 20%, respectively. The concomitant low abundances of planktonic  
341 foraminifera wwt (Fig. 2 G-H) are coherent with colder sea surface water conditions in the basin  
342 linked to Med-H<sub>TIX</sub>, lasting about 5 kyr at the IS. The pollen assemblages at the IS indicated a  
343 synchronous large expansion of open landscapes including prevalent (cold) dry steppes on land  
344 (Bertini et al., 2015).

345

#### 346 6.1.1. Possible oceanographic and atmospheric processes during terminal stadial Med-H<sub>TIX</sub>

347 The decreasing trend of temperature in latest MIS 20 is accompanied by a similar pattern of  
348 benthic  $\delta^{13}\text{C}$  (Fig. 2P) suggesting an increasing trend of water column stratification. On the other  
349 hand, the terminal stadial is not accompanied by higher  $\delta^{18}\text{O}$  values, as it may be expected during a  
350 very cold phase. The  $\delta^{18}\text{O}_{M. barleeanum}$  records a lightening of 1‰ (Fig. 2C) that could reflect the  
351 influx of lighter fresh water at the site location, possibly lowering salinity down to the sea bottom  
352 and then affecting oxygen isotope composition in the *Melonis barleeanum* tests. This process was  
353 possible due to the shallow depth (~ 100m, Aiello et al., 2015) of depositional setting of IS at this  
354 time, during glacial low sea level (Fig. 2B).

355 The occurrence of cold and fresher waters at the location of IS may reflect the arrival of melt  
356 waters coming from mountain glaciers of the close hinterland (Alpine and Apennines chains), as

357 during the last termination (Maselli et al., 2011). Alternatively, fresher water inflow into the Ionian  
358 Sea associated with North Atlantic ice melting may have occurred through the Gibraltar Strait, such  
359 a scenario being coherent to what has been observed in the western Mediterranean during recent  
360 glacial stadials correlated to Heinrich event in North Atlantic (e.g. Cacho et al., 1999; 2000; Sierro  
361 et al., 2005; Frigola et al., 2008; Martrat et al., 2014). In support of our interpretation at the IS are  
362 the data from the Balearic Sea (Quivelli, 2020); they indicate cold fresh water inflow from Atlantic  
363 or surrounding mountain glacier during the terminal stadial of MIS 20, based on the increases of  
364 polar-subpolar *N. pachyderma* and tetra-unsaturated alkenones ( $C_{37:4}$ ), and lower alkenone-derived  
365 SST, the last recording values between 8 and 11°C. Analogous evidences of Heinrich-type (Ht)  
366 events in the Alboran (Marino et al., 2018), Balearic (Girone et al., 2013; Maiorano et al., 2016b),  
367 and Ionian (Maiorano et al., 2013; Capotondi et al., 2016) basins, during the glacial MIS 12 and  
368 MIS 10, have been suggested based on calcareous plankton. Similarly, lighter planktonic  $\delta^{18}O$   
369 values and calcareous plankton assemblages suggested the arrival of Atlantic water in the central  
370 Mediterranean during main terminations of the last 70 ka (Sprovieri et al., 2012; Incarbona et al.,  
371 2013).

372 The arrival of melt waters in the Ionian basin during Med- $H_{TIX}$  has a close temporal relationship  
373 with the deposition of ice rafted debris (IRD) in the North Atlantic. Iceberg discharge and North  
374 Hemisphere ice sheet instability have been in fact documented by the IRD peaks and low  $\delta^{13}C_{benthos}$   
375 values at the sites 980 (Wright and Flower, 2002) and 983 (Kleiven et al., 2011) (see Fig. 4 O-Q),  
376 signifying time of water column stratification and shutdown of Atlantic Meridional Overturning  
377 Circulation (AMOC) (Ganopolski and Rahmstorf, 2001). We suggest that the Med- $H_{TIX}$  in the late  
378 MIS 20 at the IS is coherent with the contemporaneous oceanographic and climate signals at the  
379 southwestern Iberian margin and northern Atlantic (Fig. 4). During late MIS 20 or TIX there is no  
380 evidence of ice rafted detritus (IRD) at the mid-latitude Iberian margin, a sensitive area that  
381 recorded IRD occurrence during colder episodes of the mid-Pleistocene glacials (Stein et al., 2009;

382 Voelker et al., 2010; Rodrigues et al., 2011). However, clear indications of low salinity and cold  
383 melt water inflow have been recently documented in that area, at the Site U1385, during late MIS  
384 20 (Rodrigues et al., 2017). Low alkenone-SST (between 12 and 9°C, Fig. 4N) and higher C<sub>37:4</sub>  
385 (Fig. 4M) occurred at this time (Rodrigues et al., 2017), and a peak of *N. pachyderma* was found,  
386 centered at about 790 ka (Martin-Garcia et al., 2018), as a signal of southward migration of Polar  
387 Front. This very cold period is nearly synchronous, within the uncertainty of the different age  
388 models, with the polar-subpolar *C. pelagicus* ssp. *pelagicus* and *N. pachyderma* increases and  
389 alkenone-SST decrease at the IS (Fig. 2D) during the Med-H<sub>TIX</sub>. At the same time, the minima in  
390  $\delta^{13}\text{C}_{\text{benthos}}$  (Fig. 4L) and in log Ca/Ti patterns at the Iberian margin U1385 core (Fig. 4K) (Hodell et  
391 al., 2013, 2015) point to North Atlantic low bottom water ventilation, due to reduced North Atlantic  
392 Deep Water formation (Raymo et al., 1990, 1997), and the occurrence of a cold stadial. Such  
393 oceanographic conditions have been interpreted as similar to those occurring during the  
394 conventional Heinrich events H1 and H2, and older ones (Hodell et al., 2015). These evidences  
395 imply a clear Mediterranean response to high latitude North Atlantic climate change through  
396 oceanographic connection during mid-Pleistocene stadials.

397 The slightly warmer temperatures at the IS, compared to those recorded at the same time in the  
398 southwestern Iberian margin (Fig. 4N) and Balearic basin (8-11°C; Quivelli, 2020), may be a result  
399 of the west-east SST (and salinity) increase of MAW during its eastward route in the Mediterranean  
400 (Bélthoux, 1979; Malanotte-Rizzoli et al., 1999, 2014; von Grafenstein et al., 1999; Pinardi and  
401 Masetti, 2000). Similar temperature gradient from west (Alboran Sea, ~10-11°C, Cacho et al., 2001;  
402 Martrat et al., 2014) to east (Tyrrhenian Sea, 11-14°C, Paterne et al., 1999; eastern Mediterranean,  
403 14-16°C, Castaneda et al., 2010) was also recorded during H1.

404

405 The cold climate frame reconstructed for the Med-H<sub>TIX</sub> based on our marine proxies may have  
406 been also controlled by Atlantic-Mediterranean connection via atmospheric processes. Although the

407 past atmospheric dynamic is difficult to be known, relatively more arid climate has been inferred at  
408 the IS during H-t in MIS 20 based on pollen assemblages (Bertini et al., 2015; Maiorano et al.,  
409 2016a). This is in agreement with the general arid conditions associated to recent Heinrich events  
410 (Allen et al., 1999; Combourieu-Nebout et al., 2002; Sánchez Goñi et al., 2002; Naughton et al.,  
411 2016). Reduction of evaporation and precipitation has been also proven to occur even in the eastern  
412 Mediterranean during the Heinrich events (Bartov et al., 2003; Kwiecien et al., 2009).

413 Specifically, cold and dry Arctic air masses could have penetrated into the Ionian Sea during the  
414 winter season, similarly to what occurred during recent glacial cycles in the central and eastern  
415 Mediterranean region, and contributed, through enhanced north-westerly winds, to enhance winter  
416 deep water mixing and ventilation. Such winter deep water mixing and ventilation occurred in the  
417 Mediterranean during North Atlantic Heinrich stadials and shutdown of AMOC (Cacho et al., 1999,  
418 2000; Sierro et al., 2005; Frigola et al., 2008). The cold stadial phase during late MIS 20 in North  
419 Atlantic surface waters, as recorded by lower SST on the Iberian Margin (Fig. 4N) (Rodrigues et al.,  
420 2017), likely (i) reduced the evaporation and moisture content in air masses advected towards the  
421 Mediterranean region, promoting a cold and drier period, and (ii) induced more efficient north  
422 winter winds, and lower surface water temperature in the Ionian basin. This may have favored the  
423 proliferation of cold calcareous plankton taxa in sea surface water, as discussed above, and the arid  
424 conditions on land documented by pollen data at the IS (Bertini et al., 2015; Maiorano et al.,  
425 2016a). This seems in line with the higher aridity (Sánchez Goñi et al., 2016) recorded at the U1385  
426 (Fig. 4O). Similar atmospheric mechanisms linked to North Hemisphere ice-sheet dynamics have  
427 been suggested by Regattieri et al. (2019) to explain the high frequency climate changes displayed  
428 in the Sulmona lacustrine sediments in central Italy during MIS 19. Also, oceanic circulation and  
429 atmospheric processes related to ice-sheet dynamics in the North Atlantic have been pointed out by  
430 Nomade et al. (2019) as possible drivers of millennial-scale climate variation at the IS section  
431 during stadials and interstadials in MIS 19b-a.

432 Therefore, we believe that the Atlantic colder climate phase in late MIS 20 may have affected the  
433 Ionian basin climate by advection of subpolar low-salinity water through the Gibraltar Strait, and  
434 polar air outbreaks over the Mediterranean (e.g. Allen et al., 1999; Cacho et al., 1999, 2006;  
435 Rohling et al., 2002; Frigola et al., 2008; Rodrigo-Gámiz et al., 2011; Sprovieri et al., 2012).

436

437 Centennial-scale variability and environmental instability are recorded by marine proxies within  
438 the Med-H<sub>TIX</sub>, specifically in the oscillating SST values, with differences of temperatures up to 4°C,  
439 and in the fluctuations of key calcareous plankton taxa (Fig. 2). In more detail, *N. pachyderma*  
440 shows two main abundance peaks (Figs. 2K, 4E) that are surprisingly nearly coeval with two  
441 prominent lows in the  $\delta^{13}\text{C}_{\text{benthos}}$  at the Site U1385 (low deep water ventilation, slowdown of  
442 AMOC) (Fig. 4L). There, also SST and C<sub>37:4</sub> (Fig. 4 M-N) show a pattern with two phases of low  
443 and high values, respectively (colder and fresher/melting waters). A two-fold pattern is additionally  
444 visible in the sea level curve (Fig. 2B) which shows two minima (although in a slightly different  
445 timing due to independent age models), that would be coherent with times of higher Atlantic  
446 meltwater and polar taxa influx. On the contrary, in the middle of Med-H<sub>TIX</sub>, *G. inflata* (Fig. 2N)  
447 has fluctuating higher abundances, concurrent with fluctuating lower  $\delta^{18}\text{O}$ , indicating time of quite  
448 restored MAW inflow and periodic declines in the Atlantic meltwater arrival at the Mediterranean,  
449 possibly related to a short phase of less prominent low sea level (Fig. 2B). These data further  
450 sustain an Atlantic-Mediterranean hydrological connection even at shorter temporal scale. This  
451 variability, within the Med-H<sub>TIX</sub>, is in line with abrupt changes recorded in Mediterranean Sea  
452 during climate phases correlated to Atlantic Heinrich events (Frigola et al., 2008; Martrat et al.,  
453 2014; Bazzicalupo et al., 2018). The centennial-scale variability seems to be a regular climate  
454 pattern of Heinrich events, when investigated at very high-resolution, as sustained by the moisture  
455 spells within the cold and arid H1 event on the northwestern Iberian margin (Naughton et al., 2011,  
456 2016) and Iberian peninsula (Camuera et al., 2019), based on pollen signals. In the IS the multiple,

457 centennial-scale changes may also be associated to discontinuous meltwater influence from  
458 mountain glaciers of southern Apennines through rivers or from Alpine chain through WAC. In  
459 fact, meltwater pulses from Italian peninsula chains have been documented during last termination  
460 and specifically from Alpine glaciers in the Adriatic Sea (Maselli et al., 2011).

461

## 462 6.2 Climate variability throughout Termination IX

463 Following the Med-H<sub>TIX</sub>, the sea surface water interglacial warming, starting at about 785 ka, is  
464 preceded by an evident climate variability that is visible in the patterns of SST and selected  
465 calcareous plankton proxies (Fig. 2).

466

### 467 6.2.1 Med-BA<sub>TIX</sub> and Med-YD<sub>TIX</sub> events

468 The decrease of *C. pelagicus* ssp. *pelagicus* (Fig. 2L) and *N. pachyderma* (Fig. 2 K) and the  
469 remarkable peaks of *O. universa* (up to 25%) (Fig. 2O), together with the prominent increase of  
470 *Globorotalia inflata* (up to 80%) (Fig. 2N), represent the first signal of the climate amelioration  
471 during sea level rise, and may be associated to a Bølling-Allerød-like event (hereafter Med-BA<sub>TIX</sub>).  
472 Decrease of Cupressaceae and increase of dinocysts *S. mirabilis/hyperacanthus*, the latter known to  
473 benefit from sea surface temperature between 10 and 15 °C during winter and between 15 and 22  
474 °C during summer, confirm a climate amelioration (Maiorano et al., 2016a). This climate phase is  
475 now further supported by the alkenone-SST pattern, which records a distinct temperature increase  
476 of ca. 3°C, up to 17.6 °C, from 788.4 to 786.1 ka, resembling the Bølling-Allerød-4°C increase of  
477 the last termination in the western Mediterranean (Martrat et al., 2014). The SST profile during  
478 Med-BA<sub>TIX</sub> marks a warming in the first phase followed by a cooling trend, and does not show  
479 distinct multiple oscillations like those occurred during the BA of last termination (NGRIP, 2004)  
480 that however recorded a similar general temperature decline. Nevertheless, looking in more detail at  
481 the planktonic foraminifera key taxa within the Med-BA<sub>TIX</sub>, the opposite pattern between *O.*

482 *universa* and *G. inflata* may be observed, and could suggest that warm and freshening surface water  
483 conditions alternated in the region with period of normal salinity. *O. universa* in fact has a broad  
484 salinity tolerance and is most abundant in the vertically mixed layer and nutrient-rich areas of the  
485 low to mid-latitudes (Be, 1977; Fairbanks et al., 1982; Pujol and Vergnaud Grazzini 1995; Morard  
486 et al., 2009). This taxon, during TI, calcified in low salinity waters derived by year-round return of  
487 meltwater before and after the main climate deterioration at the H1 and YD events (Spero and  
488 Williams, 1990; Vetter et al., 2017). Therefore, we infer that the occurrence of *O. universa* at the IS  
489 in the early and late portions of Med-BA<sub>TI</sub> may be evidence of short-term climate amelioration that  
490 destabilized and melted the local ice caps of the Apennines/Alpes areas leading to increased river  
491 runoff, which caused lower sea surface salinity, increase of detrital input and nutrient into the basin,  
492 preventing enhanced proliferation of warm and oligotrophic taxa (Fig. 2 G-H). Only the  
493 opportunistic species such as *O. universa* could have found suitable environmental conditions to  
494 proliferate. On the contrary, *G. inflata*, thriving under normal salinity conditions, has higher  
495 abundance in the mid Med-BA<sub>TI</sub>, since this species undergoes vertical migrations from shallow to  
496 intermediate water depths with low vertical salinity gradients (Martinez et al., 2007). Therefore, its  
497 occurrence could attest the deepening of pycnocline and a short-term recovery of the Atlantic-  
498 Mediterranean exchange during sea level rising (Fig. 2B), in agreement with increased influx of low  
499 latitude Atlantic waters during Bølling-Allerød (Sprovieri et al., 2003; Lirer et al., 2013). Because  
500 the low-resolution pollen data at the IS do not indicate changes toward wetter condition, it is  
501 difficult to understand if the arrival of the freshwater was also supplied by wetter climate on land,  
502 but this, although at speculative level, cannot be excluded. In fact, humid climate conditions during  
503 the BA at the TI characterized the central and eastern Mediterranean areas (e.g., Combourieu-  
504 Nebout et al., 1998; Allen et al., 1999; Frisia et al., 2005; Giraudi et al., 2011; Goudeau et al., 2014)  
505 and western basin (Combourieu-Nebout et al., 2009; Bazzicalupo et al., 2018), during rapid sea



506 level rising after the H1 event and before the sapropel S1 formation (Roussakis et al., 2004;  
507 Kontiokis, 2016). Similarly, a sapropel occurs in the IS following TIX (see next section).

508 Upwards, the following and gradual SST decrease of ca 2.5°C centered at 785.8 ka, together with  
509 short-term increases of the polar-subpolar *N. pachyderma*, *C. pelagicus* ssp. *pelagicus*, and of *N.*  
510 *incompta* (Fig. 2), sustain a very short-term cool spell, before interglacial warming inception, that is  
511 interpreted as a Younger Dryas-like event (hereafter Med-YD<sub>TIX</sub>), in agreement with Maiorano et  
512 al. (2016a). A slight but distinct increase of benthic  $\delta^{13}\text{C}$  (Fig. 2P) during the Med-YD<sub>TIX</sub> marks a  
513 short-term restored sea bottom ventilation and deepening of mixed layer before the MIS 19c onset.  
514 Such environmental condition may have been driven by more efficient winter winds during an arid  
515 period, in agreement with the decreased precipitation/rainfall recorded in the central Italy during the  
516 coeval “YD” at TIX (Giaccio et al., 2015). Evidence of cold condition (abundance peak of *C.*  
517 *pelagicus* ssp. *pelagicus*) and enhanced onland erosion (higher reworked coccoliths and lithic  
518 elements) have been also recorded, based on coccolithophore assemblages, at the nearby Ionian  
519 core KC01B at the same time, following a short term warming referred to a Bølling-Allerød-type  
520 episode (Trotta et al., 2019). Similar sequence of warm and cold short term episodes just before the  
521 MIS 19c onset has been recognized in Balearic basin based on calcareous plankton assemblages and  
522 alkenone-SST (Quivelli, 2020), thus attesting high-frequency climate changes through TIX at the  
523 scale of Mediterranean basin.

524 The millennial climate variability across the MIS 20-MIS 19 deglaciation, that can be  
525 reconstructed in the IS, improves our understanding of climate evolution during terminations. Such  
526 high frequency changes seem to be a shared feature of most terminations over the last 800 ka  
527 (Barker et al., 2019), especially during times of intermediate glacial ice volume, as it is the case of  
528 MIS 20, and transitions between glacial and interglacial state (Ruddiman et al., 2016).

529

530 *6.2.2 Comparison of TIX between Ionian and Atlantic records*

531 On the whole, the new data set that we obtained through TIX (Med-BA<sub>TIX</sub> and Med-YD<sub>TIX</sub>) at  
532 the IS reinforces the working hypothesis that there should be a strong similarity between TIX and  
533 TI recorded in the Mediterranean Sea (Capotondi et al., 1999; Sbaffi et al., 2001; Asioli et al., 2001;  
534 Di Stefano and Incarbona, 2004; Siani et al., 2010, 2013; Geraga et al., 2010; Rouis-Zargouni et al.,  
535 2010; Castañeda et al., 2010; Kontakiotis, 2016; Bazzicalupo et al., 2018).

536 Although analogy with Bølling-Allerød-type and Younger-Dryas-type episodes has not been  
537 inferred so far in oceanic waters out of the Mediterranean during TIX, and because we have  
538 associated such millennial variability at the IS with North Atlantic climate, we compared our results  
539 to selected high-resolution North Atlantic sedimentary records (Fig. 4). They evidence instability in  
540 surface and subsurface waters and in climate on land during the MIS 20-19 transition (Fig. 4 H-I,  
541 K-L, O, R-S, pink bands). Specifically, oscillations may be observed in the final decreasing trend of  
542 semi-desert Mediterranean Taxa at the core U1385 (Sánchez Goñi et al., 2016) (Fig. 4O) just before  
543 the very low values occurring during MIS 19c. During this unstable phase, the  $\delta^{13}\text{C}_{\text{benthos}}$  and log  
544 Ca/Ti curves indicate short-term climate variations at the Iberian margin in terms of Atlantic Ocean  
545 deep-water ventilation/stratification, temperature, and marine productivity, respectively. Vegetation  
546 (Fig. 4 H, O) similarly records distinct, although low amplitude fluctuations before the Tajo phase;  
547 moreover, a cold spell event occurring during deglaciation is discussed in Sánchez Goñi et al.  
548 (2016) (black arrow in Fig. 4H). These oscillations (pink band in Fig. 4) likely sign the equivalent  
549 climate variability at the IS through TIX, and therefore a common high frequency variability across  
550 TIX between Iberian margin and central Mediterranean records. Similar fluctuations are shown by  
551 the  $\delta^{18}\text{O}_{\text{plankton}}$  and  $\delta^{13}\text{C}_{\text{benthos}}$  at the northern Atlantic Site 983 (pink band in Fig. 4 R-S), once more  
552 suggesting short-lived changes in temperature, salinity and deep-water ventilation, and in AMOC  
553 strength. This unstable phase has been interpreted as a result of no full recovery of ocean circulation  
554 (AMOC interglacial mode) and decrease of atmospheric CO<sub>2</sub> (Ruddiman et al., 2016; Barker et al.,  
555 2019). Therefore, a link between North Atlantic (AMOC instability) and central Mediterranean

556 climate during deglaciation MIS 20-MIS 19, similarly to MIS 20 terminal stadial phase, may be  
557 inferred. However, a full rigorous discussion on the relationships between the different climate  
558 proxies or on the timing and propagation of climate signals during TIX among the different areas  
559 needs additional investigations. In fact, the climate instability evidenced on the Iberian margin  
560 before the Tajo phase and specifically the cold spell in the Mediterranean Forest Pollen (arrow in  
561 Fig. 4H) could be correlated to the cold and dry “event 1” in the IS in the earliest MIS 19c as  
562 suggested by Asteraceae peak (Bertini et al., 2015; Marino et al., 2015; Maiorano et al., 2016a) and  
563 the reduction of Mediterranean Mesothermic Taxa (arrow in Fig. 4F).

564

### 565 6.3 The Ionian Sea “ghost sapropel”-insolation cycle 74

566 Following the Med-YD<sub>TIX</sub> event, in the lowermost climate optimum of MIS 19c (Fig. 2), the  
567 SST record reveals a quite sharp increase up to 16.5°C at 785 ka together with higher foram-wwt,  
568 very close to the mean summer insolation maximum (785.4 ka). While, total N (Fig. 2F) and nanno-  
569 wwt (Fig. 2G) do increase just above, suggesting that favorable condition (stable and oligotrophic)  
570 for the calcareous phytoplankton did occur not before 784 ka, when temperatures were higher than  
571 18.5 °C (Fig. 2D). The correlation index between total N and alkenone-SST and between nanno-  
572 wwt and alkenone-SST are quite positive, respectively +0.57 and + 0.45, and this may suggest that  
573 not only temperature but also specific trophic condition may have influenced coccolithophore  
574 productivity. The environmental conditions in the early MIS 19 at the IS have been associated  
575 (Maiorano et al., 2016a) with the occurrence of the shallow-water analogue of the “red interval”  
576 (“ghost sapropel”, oxidized sapropel, Emeis et al., 2000a), i-cycle 74 (784 ka, Lourens, 2004; 785  
577 ka, Konijnendijk et al., 2014). The very low values in  $\delta^{13}\text{C}_{C.carinata}$  also supported such interpretation  
578 (Nomade et. al., 2019) (Fig. 3I). Here, some additional elements, specifically the peculiar higher  
579 abundance peaks of selected taxa (Fig. 3 D-G), may help in revealing the double environmental  
580 signature of the ghost sapropel. During the low  $\delta^{13}\text{C}_{C.carinata}$  values, a general high *G. ruber*

581 abundance is recorded (Fig. 3G), indicative of warm oligotrophic and stratified surface waters (Bé  
582 and Hamlin, 1967; Bé, 1971; Bé and Tolderlund, 1971; Hemleben et al., 1989; Pujol and Vergnaud-  
583 Grazzini, 1995). However, the taxon shows a distinct decrease at 783.5 ka signifying a short-lived  
584 environmental change. At the same time, on the contrary, *F. profunda* and *Syracosphaera* spp. (Fig.  
585 3D, F) show a prominent peak, perfectly concurrent with the  $\delta^{13}\text{C}_{C.carinata}$  minimum (Fig. 4I).  
586 *Syracosphaera* spp. is capable to tolerate less saline and turbid surface water (Weaver and Pujol,  
587 1988; Colmenero-Hidalgo et al., 2004; Maiorano et al., 2013, 2016a, 2016b), while *F. profunda*  
588 may thrive in low light surface waters when high turbidity and nutrient availability drive the taxon  
589 upwards (Ahagon et al., 1993; Colmenero-Hidalgo et al., 2004; Maiorano et al., 2008, 2016a;  
590 Girone et al., 2013). These combined patterns at 783.5 ka suggest enhanced runoff/organic matter  
591 input from surrounding hinterland, close to insolation maximum and North Africa monsoon  
592 strengthening, promoting enhanced low oxygen conditions and organic matter preservation at the  
593 sea floor. *G. bulloides* (Fig. 2 J), that records a contemporary prominent abundance peak at 783.5 ka  
594 and an opposite pattern with respect to  $\delta^{13}\text{C}_{C.carinata}$  during sapropel deposition, may have been  
595 favored in such condition as it is an opportunistic species that proliferates in eutrophic condition.  
596 Accordingly, low total coccolithophore abundance (Fig. 2F) is likely related to turbidity increase by  
597 river terrigenous input in the Montalbano Jonico basin also supported by coarser sediment at this  
598 time (Maiorano et al., 2016a), during insolation maximum. The enhanced detrital input is a common  
599 signature observed during sapropel layers in the MJS as indicated by the increase of Al and  
600 decrease of CaO in the older sapropels i-cycles 112, 102, and i-c 86 in the lower portion of the  
601 section (Fig. 1C) (Girone et al., 2013; Maiorano et al., 2008). Starting from the  $\delta^{13}\text{C}_{C.carinata}$   
602 minimum and the decreasing trend of *G. bulloides*, stable and oligotrophic surface water conditions  
603 restored. The sharp increase of total coccolithophore assemblages and nanno-wwt (Fig. 2F)  
604 indicates warmer and more stable surface water conditions with respect to the first phase of  
605 sapropel. A very short-term peak of *Braarudosphaera bigelowii* (Fig. 3E), although with low

606 abundances, marks a low salinity spell at the end of sapropel, concurrent with increasing trend of  
607  $\delta^{13}\text{C}$  (Fig. 3I), in agreement with data of Narciso et al. (2010) for the end of sapropel S5 during MIS  
608 5.5 in the Adriatic Sea.

609 It is worth to note that recently an organic rich layer (ORL) has been recognized, for the first  
610 time, in the Balearic Sea at the TIX (Quivelli et al., 2020), supporting the basin scale event  
611 occurrence and the not in phase ORL and sapropel deposition in the western and eastern  
612 Mediterranean (Rogerson et al., 2008).

613

#### 614 *6.4 Was MIS 19c a stable full interglacial?*

615 During MIS 19c, higher SST and calcareous plankton warm water taxa, and enhanced values of  
616 total coccolith production ( $> 60$  and up to  $100$  coccoliths/g  $\times 10^7$ ) (Fig. 2D, F-H), starting from the  
617 post sapropelic layer, are evidence of climate amelioration and warmer oligotrophic sea surface  
618 waters. SST values, mainly between  $18$  and  $21.9^\circ\text{C}$  (Fig. 2D), are very similar to modern ones, and  
619 are similar to Holocene values in the region (Alkenone-SST, Emeis et al., 2000b) and in the western  
620 Mediterranean (Alkenone-SST, Cacho et al., 2001; Martrat et al., 2014). However, they are lower  
621 than in the easternmost Mediterranean (TEX86-SST, Castañeda et al., 2010) and Red Sea  
622 (Alkenone-SST, Arz et al., 2003) where Holocene SSTs are higher, as expected, ranging from about  
623  $24^\circ\text{C}$  to  $27\text{-}28^\circ\text{C}$ . A higher temperature value ( $25^\circ\text{C}$ ) has been provided by Peral et al. (2020) at  
624 the IS based on *G. ruber*-Mg/Ca estimate in one sample from MIS 19, at the level just above the  
625 end of sapropel ( $\sim 781.5$  ka). Nevertheless, the authors discuss possible biases of the Mg/Ca method  
626 in the Mediterranean Sea.

627 Two subtle phases may be distinguished at the IS during MIS 19c based on planktonic  
628 foraminifera. The first phase, starting about  $2$  ka after the end of sapropel up to  $780$  ka, was  
629 characterized by seasonal contrast with slightly lower winter temperatures, which were able to  
630 induce mixing and advection of nutrients to the surface waters, and the development of seasonal

631 DCM over warm, well stratified and oligotrophic waters in summer. This inference is based on the  
632 occurrence of *N. incompta* (Fig. 2I), and, although with very low abundances, of *G. inflata* (Fig.  
633 2N). Similar condition immediately after the end of S1 has been documented in all records from  
634 eastern Mediterranean, Adriatic and Ionian basins during the Holocene (Rohling et al., 1997;  
635 Capotondi et al., 1999; de Rijk et al., 1999; Geraga et al., 2000; 2008). The second phase of MIS  
636 19c at the IS, from about 780 ka to the end of full interglacial, is characterized by the absence of *N.*  
637 *incompta* and *G. inflata* in relation to higher abundances of *G. ruber* (Fig. 3G), suggesting that  
638 during the late MIS 19c the prevailing environmental conditions in the Ionian basin were closer to  
639 those of the modern Levantine basin than to the modern western Mediterranean Sea. Such a frame  
640 may be associated to a more permanent cyclonic regime in the Ionian Sea (Fig. 1D) leading the  
641 northern internal border of the basin under the direct influence of poor-nutrient LIW (Civitarrese et  
642 al., 2010). This is consistent with the modern regional distribution of *G. inflata* that it is absent in  
643 the northern Ionian Sea (Mallo et al., 2017; Di Donato et al., 2019) but occurs in the southern basin  
644 following the path of Atlantic waters that, under cyclonic regime, does not arrive in the northern  
645 sector of the basin. The distribution of *G. inflata*, during MIS 19c seems similar to its pattern during  
646 Holocene in the northern Ionian Sea. There, during the last 6 kyr, starting from about 2 ka after the  
647 end of S1 deposition (like at the IS after sapropel i-cycle 74), *G. inflata* is absent, with the exception  
648 of short incursions during period of reversed circulation (Di Donato et al., 2019), which depends  
649 upon variations in the atmospheric forcing on cyclonic-anticyclonic oceanographic regime (Poulin  
650 et al., 2012).

651 Higher frequency variable environmental conditions may be distinguished in the uppermost  
652 surface waters looking in more details at the patterns of the main climate proxies during MIS 19c.  
653 Specifically, six oscillations in about 11 kyr may be observed in total N and SST curves (Fig. 2D,  
654 F). These in-phase fluctuations, if smoothed-out by a 5-points running average, appear as three  
655 main warmer phases (violet arrows in Fig. 2D, F-G). The curve of Mediterranean Mesothermic taxa

656 at the IS (Fig. 2 E), although at low resolution, seems to record a similar pattern as well, almost in  
657 phase with the three higher alkenone-SST in MIS 19c, pointing to an in-phase high climate  
658 variability in both marine and continental settings, and then implying both oceanographic and  
659 atmospheric processes. The main increases of Mediterranean Mesothermic taxa at the IS (Fig. 2E)  
660 may be linked to southward westerly shift and higher winter precipitation in south Europe and  
661 Mediterranean basin (Wagner et al., 2019), perhaps in analogy to processes operating like the  
662 modern or recent North Atlantic Oscillation mode (Xoplaki et al., 2003; Moreno et al., 2002, 2004,  
663 2005; Hurrell et al., 2004; Roberts et al., 2008; Fletcher et al., 2009; Ulbrich et al., 2012). The main  
664 increases of nanno-wwt in sea surface water (Fig. 2G) would be the result of increased inflow of  
665 warm tropical-subtropical waters through the Gibraltar Strait toward central Mediterranean.

666 Additional seasonal climate insights derive from the distribution pattern of foraminifer  
667 *Trilobatus sacculifer* (Fig. 2 H), a tropical-subtropical taxon (Bé, 1977; Vincent and Berger, 1981)  
668 that has a peculiar occurrence in MIS 19c, showing multiple oscillations and an opposite  
669 distribution with respect to *G. ruber* (Fig. 2S). This pattern could be related to low seasonality and  
670 milder winters (Bé and Hutson, 1977; Fraile et al., 2008; Hemleben et al., 1989; Vincent and Berger,  
671 1981), or to short term periods of relative less humid conditions; this in accordance with findings  
672 during the mid Pleistocene interglacial MIS 11 (Maiorano et al., 2016b; Marino et al., 2018) and  
673 Holocene in the Mediterranean and Red Sea basins (Piva et al., 2008; Edelman-Furstenberg et al.,  
674 2009). The inferred periods of less humid conditions during the two major peaks of *T. sacculifer* are  
675 supported by the correlative phases of reduction of Mediterranean Mesothermic taxa, especially in  
676 the upper MIS 19c (Fig. 2).

677 The unstable climate character of MIS 19c climate has been recorded in the high-resolution  
678 records from central Italy Sulmona sediments and at the U1385, and related to North Atlantic  
679 oceanic-atmospheric-climate processes (Sánchez Goñi et al., 2016; Regattieri et al., 2019). In  
680 particular, three main increases of the Mediterranean Forest Pollen during Tajo phase were detected

681 on the Iberian margin similarly to what occurs in the MIS 19c at the IS, whereas a decoupled  
682 response between terrestrial (pollen, Fig. 4 H, O) and marine ( $C_{37:4}$ , alkenone-SST, Fig. 4 M-N)  
683 signals (the latter recording a certain stability throughout the entire full interglacial) was evidenced  
684 at Site U1385. This was explained as a direct and synchronous response of Iberian vegetation to  
685 northern Atlantic climate via atmospheric process (like at the IS), whereas sea surface temperatures  
686 remained almost stable at the location of core U1385 due to the effect of warm retaining of  
687 subtropical gyre (Repschläger et al., 2015), even during reduced Mediterranean Forest Pollen (Fig.  
688 4H) (Sánchez Goñi et al., 2016). It is possible that during MIS 19c the common feature of  
689 vegetation patterns, as recorded in IS and Iberian margin, was a shared response to atmospheric  
690 processes that in concert also influenced the marine proxies (SST, total N and coccolithophore wwt)  
691 in the Ionian Sea, contrary to what happened in the Atlantic waters west of Iberia.

692

#### 693 *6.5 The stadial-interstadial phases in MIS 19b-a*

694 The first signal of climate deterioration at the end of full interglacial MIS 19c occurs at ~773-774  
695 ka when alkenone-SST displays a prominent drop of about 8-9°C with a minimum of 12.1°C at  
696 772.8 ka; this temperature drop is even stronger than in Med-H<sub>TIX</sub>. Warm water taxa decrease at the  
697 same time (Fig. 2 D, G-H), thus marking the first significant cooling and the substage MIS 19b,  
698 synchronous with the first enrichment of  $\delta^{18}O$  values (Figs. 2, 4). MIS 19b is very distinctive in the  
699 IS, being very close to the Ar/Ar dated V4 and  $^{10}Be/^{9}Be$  peak (interpreted as the Earth magnetic  
700 field collapse during the Matuyama-Brunhes reversal, Simon et al., 2017), and associated to the  
701 beginning of polar ice-sheet increase and instability (Maiorano et al., 2016a), synchronously with  
702 the first IRD occurrence after full interglacial MIS 19 in northern Atlantic (Kleiven et al., 2011). At  
703 this time, the Mediterranean Mesothermic taxa (Fig. 2E) decrease while the steppic and halophyte  
704 vegetation advance at the IS, highlighting cold and arid condition over the central Mediterranean  
705 hinterland (Bertini et al., 2015). A quite concurrent slight increase of semi-desert vegetation



706 centered at ~772.6 ka (Fig. 4O) and decrease of Mediterranean Forest Pollen (Fig. 4H) occur at the  
707 core U1385, suggestive of a cooling/arid episode on the southwestern Iberian. On the other hand, no  
708 coeval noticeable variation occurs in the alkenone records at the Site U1385 (Fig. 4M-N). Our data  
709 set at the IS seems to underline that at the time of MIS 19b the response of calcareous plankton  
710 (Fig. 2F-G, L) and alkenone-SST (Fig. 2 D) is clearly in phase with the vegetation response (Fig. 2  
711 E), and both are in phase with the pollen data at the Iberian margin (Fig. 4M, O). While at Site  
712 U1385 the subtropical gyre was responsible for the still presence of warm waters, a southward  
713 influx of cold and dry arctic air masses towards the IS location promoted efficient cooling of both  
714 marine and terrestrial environments, maybe more efficiently than during Med-H<sub>TIX</sub>. It is possible  
715 that continental cold and dry air flux by enhanced Siberia High (SH) pressure had a role in the  
716 central Mediterranean at this time. An equivalent pattern is seen in the Holocene record in the  
717 eastern Mediterranean, where intensified SH has been suggested for the cold and dry spell at 8.2 ka  
718 (Pross et al., 2009). Accordingly, rapid transmission of high latitude Arctic/North Atlantic  
719 perturbations to the northwestern and eastern Mediterranean has been documented in several studies  
720 for recent and past severe cold events (Leaman and Scott, 1991; Mariolopoulos, 1961; Poulos et al.,  
721 1997; Rohling et al., 1998, 2002, 2009; Casford et al., 2001; Melki et al., 2009) and they would  
722 support our environmental reconstruction for MIS 19b.

723 Above MIS 19b, the most prominent feature of climate evolution in the IS is the occurrence of  
724 multiple oscillations in all climate proxies (Figs 2, 4) that are related to the reestablishment of  
725 millennial-scale variability and, presumably, of the bipolar seesaw (Tzedakis et al., 2012). This  
726 climate trend toward the glacial stage 18 onset is very well recorded at the IS, as widely discussed  
727 in Nomade et al. (2019, to whom we refer) based on oxygen and carbon isotopes, and is now finely  
728 improved by our new data set (Fig. 2). The three distinct interstadial oscillations during MIS 19a  
729 (19a-1, 19a-2, and 19a-3) at the IS are evidenced by the impressive parallel fluctuating  
730 increase/decrease of alkenone-SST pattern as well as of warm and cold water taxa indicators (Figs.

731 2-4). In addition, total coccolith production increased during warmer and oligotrophic interstadial  
732 phases; these were characterized by lower deepwater ventilation (lower  $\delta^{13}\text{C}$ , Fig. 2T), even if not  
733 as pronounced as during sapropel deposition in MIS 19c (Fig. 2). The inceptions of these  
734 interstadials were characterized not only by sudden warming but also by abrupt changes in the  
735 surface hydrological regime in the basin. This paleoenvironmental reconstruction is based on the  
736 sharp increases of *O. universa* at the beginning of the interstadials 19a-1 and 19a-2, when the SST  
737 did not reach maximum values, the  $\delta^{13}\text{C}$  was lower than in the second half of interstadials, and the  
738 stadial-interstadial  $\delta^{18}\text{O}$  lightening shifts are very sharp. We believe that abrupt climate  
739 amelioration at the onset of interstadials would have destabilized local mountain glaciers resulting  
740 in the return of local meltwater input into the basin. This frame reflects superimposed local process  
741 on global climate signals and definitively sustains the local freshwater discharge hypothesized by  
742 Nomade et al. (2019) to explain the very rapid (<200 years) and high amplitude stadial-interstadial  
743 oscillations described by the  $\delta^{18}\text{O}$  record during MIS 19a. Wetter climate conditions on land, as  
744 suggested by pollen assemblages at the IS (Fig. 2E), contributed to increase the freshening  
745 conditions of sea surface waters leading to the reduction of bottom water ventilation (low benthic  
746  $\delta^{13}\text{C}$ ), in agreement with the higher precipitation over the Italian peninsula documented by both the  
747 Pianico-Sellere and Sulmona paleolake records (Moscariello et al., 2000; Rossi, 2003; Giaccio et  
748 al., 2015; Nomade et al., 2019). Such a pattern points to a marked correspondence between  
749 terrestrial and marine records and then between atmospheric and oceanographic processes during  
750 MIS 19a in the central Mediterranean.

751 Among the interstadials, 19a-2 appears as the warmest, in agreement with higher SST and the  
752 occurrence of tropical *T. sacculifer* (Fig. 2 H), suggesting the establishment of surface water  
753 condition similar to the MIS 19c climate optimum. Low eccentricity combined with weak insolation  
754 maximum and obliquity minimum (Fig. 2A) could have favored the establishment of the year-round

755 condition of low seasonal contrast. In the final part of MIS 19a, the shallowing trend of the  
756 Montalbano basin has been reconstructed (Ciaranfi et al., 2010, and references therein),  
757 simultaneous with a global sea level lowering trend (Fig. 2B). The lower depths during stadials of  
758 MIS 19a were characterized by increased turbidity in surface water, as evidenced by higher *H.*  
759 *carteri* abundances (Fig. 2M) that, like during glacial MIS 20, increase in relation to times of lower  
760 sea level, which enhances erosion on land and inorganic input influx into the basin. Associated to  
761 these events may be the supply of nutrients to the sea. The general increasing trend of the  
762 opportunistic *G. bulloides* in the upper section (Fig. 2J) is in fact evidence of enhanced nutrient  
763 availability likely of on land origin. A cooling trend toward the top of the study section up to the  
764 MIS 18 glacial onset at 757 ka (Nomade et al., 2019) co-occurs, and is sustained by the heavier  
765 values of  $\delta^{18}\text{O}$  together with the increased occurrence of cold water taxa *C. pelagicus* ssp. *pelagicus*  
766 and *N. pachyderma* and decreasing trend of wwt and total N (Fig. 2).

767

## 768 **7. Conclusions**

769 The high-resolution data set obtained at the Ideale section based on alkenone-SST and calcareous  
770 plankton analyses, combined with the available high-resolution  $\delta^{18}\text{O}$  and  $\delta^{13}\text{C}$  records, evidence  
771 orbital-suborbital climate oscillations which delineate a detailed climatostratigraphic frame through  
772 late MIS 20 to early MIS 18. This is a crucial time interval of the mid-Pleistocene transition that  
773 includes the Lower-Middle Pleistocene chronostratigraphic boundary close to the Matuyama-  
774 Brunhes paleomagnetic reversal associated to MIS 19c/MIS 19b.

775 The alkenone-SST, that is the first record in the Mediterranean Sea in this time interval,  
776 distinctly records the climate pattern across MIS 20-18 and makes it possible to identify substages  
777 and shorter-term climate variations. The oscillations of SST and calcareous plankton key taxa  
778 confirm that there exists a strong analogy between TIX and last deglaciation, and sustain the  
779 identification of Heinrich-type, BA-type and YD-type events during TIX, here named Med-H<sub>TIX</sub>,

780 Med-BA<sub>TIX</sub>, and Med-YD<sub>TIX</sub>, respectively. The recognition of these episodes improves our  
781 knowledge on the climate evolution during terminations of last 800 kyr. Multiple very short-term  
782 SST fluctuations characterized the Med-H<sub>TIX</sub> event confirming the regular climate pattern of  
783 Heinrich events when studied at very high-resolution. The Med-BA<sub>TIX</sub> is marked by higher SST at  
784 the beginning followed by a long cooling trend towards the Med-YD<sub>TIX</sub> episode. The  
785 paleoenvironmental conditions during the sapropelic layer occurring at the beginning of interglacial  
786 19, during insolation maximum (i-c 74), are characterized by centennial-scale internal variability,  
787 synchronously displayed by the multiple proxies.

788 Unstable conditions in MIS 19c have been discovered, with three main phases of increased SST,  
789 calcareous plankton warm water taxa. Higher frequency variability has been revealed by the  
790 uppermost surface water proxies and corresponds to multiple pulses of tropical-subtropical water  
791 inflow into the basin and variable hydrological cyclonic regime in the Ionian Sea. The distinct  
792 climate fluctuations in MIS 19b-a interval are the result of global climate changes being correlatable  
793 worldwide, but they are emphasized by the location of the IS close to Italian hinterland, suited to  
794 record local changes in freshwater/detrital/nutrient inputs, influencing the calcareous plankton taxa,  
795 making them powerful proxies for detailed environmental reconstruction.

796 Comparison of our results with selected mid- and high-latitude North Atlantic marine and  
797 terrestrial climate proxies, pinpoints to the occurrence of similar climate oscillations, in spite of the  
798 different age models among sites and the influence of different control factors in diverse  
799 oceanographic settings. Data suggest that the North Atlantic and polar climate dynamics strongly  
800 affected the climate evolution at the IS location and that atmospheric processes, other than  
801 oceanographic, may have had a prominent role on marine and terrestrial environments in central  
802 Mediterranean. The clarification of timing and areal propagation of climate signals through  
803 oceanographic and/or atmospheric connection requires additional high-resolution multi-proxy  
804 studies from different regions in well-constrained chronological frameworks.

805

## 806 **Acknowledgments**

807 This research was financially supported by Università degli Studi di Bari Aldo Moro, Fondi di  
808 Ateneo P. Maiorano, 2016 and benefited of instrumental upgrades from “Potenziamento Strutturale  
809 PONa3\_00369 dell'Università degli Studi di Bari, Laboratorio per lo Sviluppo Integrato delle  
810 Scienze e delle TECnologie dei Materiali Avanzati e per dispositivi innovativi (SISTEMA)”.

811

## 812 **Supplementary data**

813 Supplementary data to this article can be found online at ...

814

## 815 **References**

- 816 Abrantes, F., Voelker, A.H.L., Sierro, F.J., Naughton, F., Rodrigues, T., Cacho, I., Ariztegui, D., Brayshaw,  
817 D., Sicre, M.A., Batista, L., 2012. Paleoclimate variability in the Mediterranean region. In: Lionello P.  
818 (ed) *The climate of the Mediterranean region: from the past to the future*. Elsevier, Amsterdam, pp 1-86.  
819 doi:10.1016/B978-0-12-416042-2.00001-X.
- 820 Aiello, G., Barra, D., Parisi, R., 2015, Lower-Middle Pleistocene ostracod assemblages from the Montalbano  
821 Jonico section (Basilicata, southern Italy). *Quaternary International* 383, 47-73,  
822 <http://dx.doi.org/10.1016/j.quaint.2014.11.010>.
- 823 Ahagon, N., Tanaka, Y., Ujiie, H., 1993. *Florisphaera profunda*, a possible nannoplankton indicator of late  
824 Quaternary changes in sea-water turbidity at the northwestern margin of the Pacific. *Mar. Micropaleontol.*  
825 22, 255-273.
- 826 Allen, J. R., Brandt, U., Brauer, A., Hubberten, H. W., Huntley, B., Keller, J., Nowaczyk, N. R., 1999. Rapid  
827 environmental changes in southern Europe during the last glacial period. *Nature* 400(6746), 740
- 828 Alonso-García, M., Sierro, F.J., Flores, J.A., 2011. Arctic front shifts in the subpolar North Atlantic during  
829 the Mid-Pleistocene (800–400 ka) and their implications for ocean circulation. *Palaeogeogr.*  
830 *Palaeoclimatol. Palaeoecol.* 311 (3–4), 268–280. <https://doi.org/10.1016/j.palaeo.2011.09.004>.
- 831 Amore, F.O., Flores, J.A., Voelker, A.H.L., Lebreiro, S.M., Palumbo, E., Sierro, F.J., 2012. A Middle  
832 Pleistocene Northeast Atlantic coccolithophore record: paleoclimatology and paleoproductivity aspects.  
833 *Mar. Micropaleontol.* 90-91, 44-59.
- 834 André, A., Weiner, A., Quillévéré, F., Aurahs, R., Morard, R., Douady, C.J., de Garidel-Thoron, T.,  
835 Escarguel, G., de Vargas, C., Kucera, M., 2013. The cryptic and the apparent reversed: lack of genetic  
836 differentiation within the morphologically diverse plexus of the planktonic foraminifer *Globigerinoides*  
837 *sacculifer*. *Paleobiology* 39 (1), 21-39.
- 838 Arz, H. W., Lamy, F., Pätzold, J., Müller, P. J., Prins, M., 2003. Mediterranean moisture source for an Early  
839 Holocene humid period in the northern Red Sea, *Science*, 300, 118-121, doi:10.1126/science.1080325.
- 840 Asioli, A., Trincardi, F., Lowe, J.J., Ariztegui, D., Langone, L., Oldfield, F., 2001. Submillennial-scale  
841 climatic oscillations in the central Adriatic during the Late glacial: palaeoceanographic implications.  
842 *Quat. Sci. Rev.* 20, 1201-1221.
- 843 Aurahs, R., Treis, Y., Darling, K., Kucera, M., 2011. A revised taxonomic and phylogenetic concept for the  
844 planktonic foraminifer species *Globigerinoides ruber* based on molecular and morphometric evidence.  
845 *Mar. Micropaleontol.* 79, 1-14.
- 846 Azzaroli, A., Perno, U., Radina, B., 1968. Note illustrative della Carta Geologica d'Italia alla scala  
847 1:100.000, Foglio 188 Gravina di Puglia: Servizio Geologico Italiano, 57 pp.

848 Bárcena, M. A., Flores, J. A., Sierro, F. J., Pérez-Folgado, M., Fabres, J., Calafat, A., Canals, M., 2004.  
849 Planktonic response to main oceanographic changes in the Alboran Sea (Western Mediterranean) as  
850 documented in sediment traps and surface sediments. *Marine Micropaleontology* 53(3-4), 423-445.  
851 Barker, S., Knorr, G., Conn, S., Lordsmith, S., Newman, D., Thornalley, D., 2019. Early interglacial legacy  
852 of deglacial climate instability. *Paleoceanography, Paleoclimatology*. doi: 10.1029/2019PA003661.  
853 Bartov, Y., Goldstein, S. L., Stein, M., Enzel Y., 2003. Catastrophic arid episodes in the eastern  
854 Mediterranean linked with the North Atlantic Heinrich events, *Geology* 31, 439-442.  
855 Bassinot, F., Labeyrie, L., Vincent, E., Quidelleur, X., Shackleton, N., and Lancelot, Y., 1994, The  
856 astronomical theory of climate and the age of the Brunhes-Matuyama magnetic reversal. *Earth and  
857 Planetary Science Letters* 126 (1-3), 91-108, doi:10.1016/012-821X(94)90244-5.  
858 Batistić, M., Viličić, D., Kovačević, V., Jasprica, N., Lavignec, H., Carića, M., Garić, R., Cara, A., 2017,  
859 Winter phytoplankton blooms in the offshore south Adriatic waters (1995-2012) regulated by  
860 hydroclimatic events: Special emphasis on the exceptional bloom of 1995. *Biogeosciences Discuss.*  
861 <https://doi.org/10.5194/bg-2017-205>  
862 Baumann, K.-H., Andruleit, H., Samtleben, C., 2000. Coccolithophores in the Nordic Seas: comparison of  
863 living communities with surface sediment assemblages. *Deep Sea Res. Part II* 47, 1743-1772.  
864 Baumann, K.-H., Bockel, B., Frenz, M., 2004. Coccolith contribution to South Atlantic carbonate  
865 sedimentation. In: Thierstein, H.R., Young, J. (Eds.), *Coccolithophores: From Molecular Processes to  
866 Global Impact*. Springer, Berlin, pp. 367-402.  
867 Baumann, K.H., Andruleit, H., Böckel, B., Geisen, M., Kinkel, H., 2005. The significance of extant  
868 coccolithophores as indicators of ocean water masses, surface water temperature, and paleoproductivity: a  
869 review. *Paläontol. Z.* 79, 93-112.  
870 Bazzicalupo, P., Maiorano, P., Gironi, A., Marino, M., Combourieu-Nebout, N., Incarbona, A., 2018. High-  
871 frequency climate fluctuations over the last deglaciation in the Alboran Sea, Western Mediterranean Sea:  
872 evidence from calcareous plankton assemblages. *Palaeogeography, Palaeoclimatology, Palaeoecology*  
873 506, 226-241.  
874 Bé, A.W.H., 1971. Winter distribution of planktonic foraminifera between the Grand Banks and the  
875 Caribbean. *Micropalaeontology* 17 (1), 31-42.  
876 Bé, A.W.H., 1977. An ecological, zoogeographic and taxonomic re view of recent planktonic foraminifera.  
877 In: Ramsay, A.T.S. (Ed.) *Oceanic Micropaleontology* vol. 1. Academic Press, London, p. 1.  
878 Bé, A.W.H., Hamlin, W.H., 1967. Ecology of recent planktonic foraminifera. *Micropaleontology* 13, 87-100.  
879 Bé, A.W.H., Tolderlund, D.S., 1971. Distribution and ecology of living planktonic foraminifera in surface  
880 waters of the Atlantic and Indian Oceans. In: Funnell, B.M., Riedel, W.R. (Eds.), *The Micropaleontology  
881 of the Oceans*, pp. 105-149.  
882 Bé, A.W.H., Hutson, W.H., 1977. Ecology of Planktonic Foraminifera and Biogeographic Patterns of Life  
883 and Fossil Assemblages in the Indian Ocean. *Micropaleontology* 23(4). The Micropaleontology Project.,  
884 Inc.: 369. DOI: 10.2307/1485406.  
885 BÉlthoux, G.P., 1979. Budgets of the Mediterranean Sea: their dependence on the local climate and on the  
886 characteristics of the Atlantic waters. *Ocean. Acta* 2, 157-163.  
887 Bertini, A., Toti, F., Marino, M., Ciaranfi, N., 2015, Vegetation and climate across the Early-Middle  
888 Pleistocene transition at the Montalbano Jonico section (southern Italy): Quaternary International 383, 74-  
889 88, <http://dx.doi.org/10.1016/j.quaint.2015.01.003>.  
890 Bignami, F., Sciarra, R., Carniel, S., Santoleri, R., 2007, Variability of Adriatic Sea coastal turbid waters  
891 from SeaWiFS imagery. *J. Geophys. Res.* 112, C03S10, doi:10.1029/2006JC003518.  
892 Boeckel, B., Baumann, K.-H., 2004. Distribution of coccoliths in surface sediments of the south-eastern  
893 South Atlantic Ocean: ecology, preservation and carbonate contribution. *Marine Micropaleontol.* 51 (3-4),  
894 301-320.  
895 Boenzi, F., Capolongo, D., Gallicchio, S., Di Pinto, G., 2014. Morphostructure of the Lucania Apennines  
896 front between the Basento and Salandrella rivers (Southern Italy). *J. Maps* 10 (3), 478–486.  
897 Bonomo, S., Cascella, A., Alberico, I., Lirer, F., Vallefucio, M., Marsella, E., Ferraro, L., 2018. *Marine  
898 Micropaleontology*, 142, 67-91, <https://doi.org/10.1016/j.marmicro.2018.06.003>  
899 Brückner, H., 1980a. Marine Terrassen in Südtalien. Eine quartärmorphologische Studie über das  
900 Küstentiefland von Metapont. *Düsseldorfer Geographische Schriften*, 14, 235 pp.

- 901 Brückner H., 1980b. - Flußterrassen und flußtäler im Küstentiefland von Metapont (Süditalien) und ihre  
 902 Beziehung zu Meeresterrassen. *Düsserdolfer Geographische Schriften*, 15, 5-32.
- 903 Cacho, I., Grimalt, J.O., Pelejero, C., Canals, M., Sierro, F.J., Flores, J.A., Shackleton, N.J., 1999.  
 904 Dansgaard-Oeschger and Heinrich event imprints in the Alboran Sea paleotemperatures.  
 905 *Paleoceanography* 14, 698-705.
- 906 Cacho, I., Grimalt, J.O., Sierro, F.J., Shackleton, N.J., Canals, M., 2000. Evidence for enhanced  
 907 Mediterranean thermohaline circulation during rapid climatic coolings. *Earth Planet. Sci. Lett.* 183, 417-  
 908 429
- 909 Cacho, I., Grimalt, J.O., Canals, Saffi, M., L., Shackleton, J., Schonfeld, J., Zahn, R., 2001. Variability of  
 910 the western Mediterranean Sea surface temperature during the last 25,000 years and its connection with  
 911 the Northern Hemisphere climatic change. *Paleoceanography* 16(1): 40–52. DOI: 10.1029/SP010
- 912 Cacho, I., Shackleton, N., Elderfield, H., Sierro, F.J., and Grimalt, J.O. 2006. Glacial rapid variability in  
 913 deep-water temperature and  $\delta^{18}\text{O}$  from the Western Mediterranean Sea, Quaternary. *Sci. Rev.* 25, 3294-  
 914 3311.
- 915 Camuera, J., Jiménez-Moreno, G., Ramos-Román, M. J., García-Alix, A., Jiménez-Espejo, F., Toney, J. L.,  
 916 Anderson, R. S., Webster, C., 2019. Climatic subdivision of Heinrich Stadial 1 based on centennial-scale  
 917 paleoenvironmental changes observed in the western Mediterranean area, *Clim. Past Discuss.*,  
 918 <https://doi.org/10.5194/cp-2019-130>.
- 919 Capotondi, L., Borsetti, A.M., Morigi, C., 1999. Foraminiferal ecozones, a high-resolution proxy for the late  
 920 Quaternary biochronology in the central Mediterranean Sea. *Mar. Geol.* 153, 253-274.
- 921 Capotondi, L., Girone, A., Lirer, F., Bergami, C., Verducci, M., Vallefucio, M., Afferri, A., Ferraro, L.,  
 922 Pelosi, N., De Lange, G.J., 2016. Central Mediterranean Mid-Pleistocene paleoclimatic variability and its  
 923 connection with global climate. *Palaeogeogr. Palaeoclimatol. Palaeoecol.* 442, 72–83.
- 924 Casford, J.S.L., Abu-Zied, R., Rohling, E.J., Cooke, S., Boessenkool, K.P., Brinkhuis, H., De Vries, C.,  
 925 Wefer, G., Geraga, M., Papatheodorou, G., Croudace, I., Thomson, I., Lykousis, V., 2001. Mediterranean  
 926 climate variability during the Holocene. *Mediterranean Marine Science* 2/1, 45-55.
- 927 Casford, J. S. L., Rohling, E. J., Abu-Zied, R. H., Fontanier, C. F., Jorissen, J., Leng, M. J., Schmiedl, G.,  
 928 Thomson, J., 2003, A dynamic concept for eastern Mediterranean circulation and oxygenation during  
 929 sapropel formation, *Palaeogeogr. Palaeoclimatol. Palaeoecol.* 190, 103-119.
- 930 Casnedi, R., 1988. La Fossa bradanica: origine, sedimentazione e migrazione. *Memorie Società Geologica*  
 931 *Italiana* 41, 439-448.
- 932 Castañeda, I.S., Schefuß, E., Pätzold, J., Sinninghe Damsté, J.S., Weldeab, S., Schouten, S., 2010.  
 933 Millennial-scale sea surface temperature changes in the eastern Mediterranean (Nile River Delta region)  
 934 over the last 27,000 years. *Paleoceanography* 25 (1).
- 935 Channell, J.E.T., Hodell, D.A., Singer, B.S., and Xuan, C., 2010, Reconciling astrochronological and  
 936  $^{40}\text{Ar}/^{39}\text{Ar}$  ages for the Matuyama-Brunhes boundary in the late Matuyama Chron. *Geochemistry,*  
 937 *Geophysics, Geosystems*, v. 11, Q0AA12, <http://dx.doi.org/10.1029/2010GC003203>.
- 938 Ciaranfi, N., D'Alessandro, A., 2005, Overview of the Montalbano Jonico area and section: a proposal for a  
 939 boundary stratotype for the lower-middle Pleistocene, southern Italy Foredeep: *Quaternary International*  
 940 131, 5-10.
- 941 Ciaranfi, N., Lirer, F., Lirer, L., Lourens, L.J., Maiorano, P., Marino, M., Petrosino, P., Sprovieri, M.,  
 942 Stefanelli, S., Brillì, M., Girone, A., Joannin, S., Pelosi, N., Vallefucio, M., 2010, Integrated stratigraphy  
 943 and astronomical tuning of the Lower-Middle Pleistocene Montalbano Jonico land section (southern  
 944 Italy): *Quaternary International* 210, 109-120.
- 945 Civitarese, G., Gačić, M., Lipizer, M., Eusebi Borzelli, G. L., 2010, On the impact of the Bimodal  
 946 Oscillating System (BiOS) on the biogeochemistry and biology of the Adriatic and Ionian Seas (Eastern  
 947 Mediterranean), *Biogeosciences* 7, 3987–3997, doi:10.5194/bg-7-3987-2010
- 948 Colmenero-Hidalgo, E., Flores, J.A., Sierro, F.J., Barcena, M.A., Lowemark, L., Schonfeld, J., Grimalt, J.O.,  
 949 2004. Ocean surface water response to short-term climate changes revealed by coccolithophores from the  
 950 Gulf of Cadiz (NE Atlantic) and Alboran Sea (W Mediterranean). *Palaeogeogr. Palaeoclimatol.*  
 951 *Palaeoecol.* 205, 317-336.
- 952 Combourieu Nebout, N., Paterne, M., Turon, J. L., Siani, G., 1998. A high-resolution record of the last  
 953 deglaciation in the Central Mediterranean Sea: Palaeovegetation and Palaeohydrological evolution,  
 954 *Quaternary Sci. Rev.* 17, 303-317.

955 Combourieu Nebout, N., Turon, J. L., Zahn, R., Capotondi, L., Londeix, L., Pahnke, K., 2002. Enhanced  
956 aridity and atmospheric high-pressure stability over the western Mediterranean during the North Atlantic  
957 cold events of the past 50 ky. *Geology* 30(10), 863-866.

958 Combourieu Nebout, N., Peyron, O., Dormoy, I., Desprat, S., Beaudoin, C., Kotthoff, U., Marret, F., 2009.  
959 Rapid climatic variability in the West Mediterranean during the last 25000 years from high-resolution  
960 pollen data. *Clim. Past* 5, 503–521

961 D'Alessandro, A., La Perna, R., Ciaranfi, N., 2003, Response of macrobenthos to changes in  
962 paleoenvironment in the Lower-Middle Pleistocene (Lucania Basin, southern Italy). *Il Quaternario* 16,  
963 167-182.

964 Darling, K.F., Kucera, M., Kroon, D., Wade, C.M., 2006. A resolution for the coiling direction paradox in  
965 *Neoglobobulimina papyroderma*. *Paleoceanography* 21 (2), PA2011.

966 De Rijk, S., Rohling, E.J., Hayes, A., 1999, Onset of climatic deterioration in the eastern Mediterranean  
967 around 7 ky BP; micropalaeontological data from Mediterranean sapropel interruptions. *Mar. Geol.* 153,  
968 337-343.

969 Di Donato, V., Insinga, D.D., Iorio, M., Molisso, F., Rumolo, P., Cardines, C., Passaro, S., 2019. The  
970 palaeoclimatic and palaeoceanographic history of the Gulf of Taranto (Mediterranean Sea) in the last 15  
971 ky. *Global and Planetary Change* 172, 278–297. <https://doi.org/10.1016/j.gloplacha.2018.10.014>.

972 Di Stefano, E., Incarbona, A., 2004. High-resolution paleoenvironmental reconstruction of the ODP-963D  
973 Hole (Sicily Channel) during the last deglaciation, based on calcareous nannofossils. *Mar.*  
974 *Micropaleontol.* 52, 241-254.

975 Doglioni, C., Tropeano, M., Mongelli, F., Pieri, P., 1996, Middle-Late Pleistocene uplift of Puglia: an  
976 “anomaly” in the Apenninic foreland. *Memorie della Società Geologica Italiana* 51, 101-117.

977 Edelman-Furstenberg, Y., Almogi-Labin, A., Hemleben, C., 2009. Palaeoceanographic evolution of the  
978 central Red Sea during the late Holocene. *The Holocene* 19, 117-127.  
979 <https://doi.org/10.1177/0959683608098955> .

980 Elderfield, H., Ferretti, P., Greaves, M., Crowhurst, S., McCave, I.N., Hodell, D., Piotrowski, A.M., 2012.  
981 Evolution of ocean temperature and ice volume through the mid-Pleistocene climate transition. *Science*  
982 337, 704-709.

983 Emanuele, D., Ferretti, P., Palumbo, E., and Amore, F.O., 2015. Sea-surface dynamics and  
984 palaeoenvironmental changes in the North Atlantic Ocean (IODP Site U1313) during Marine Isotope  
985 Stage 19 inferred from coccolithophore assemblages: Palaeogeography, Palaeoclimatology,  
986 Palaeoecology 430, 104-117.

987 Emeis, K., Sakamoto, T., Wehausen, R., Brumsack, H.J., 2000a. The sapropel record of the eastern  
988 Mediterranean Sea - results of Ocean Drilling Program Leg 160: Palaeogeography, Palaeoclimatology,  
989 Palaeoecology 158, 371-395.

990 Emeis, K.-C., Struck, U., Schulz, H.-M., Bernasconi, S., Sakamoto, T., Martinez-Ruiz, F., 2000b.  
991 Temperature and salinity of Mediterranean Sea surface waters over the last 16 000 years: constraints on  
992 the physical environment of S1 sapropel formation based on stable oxygen isotopes and alkenone  
993 unsaturation ratios, Palaeogeogr. Palaeoclimatol. 158, 259-280.

994 Fairbanks, R.G., Sverdrup, M., Free, R., Wiebe, P.H., Bé, A.W.H., 1982. Vertical distribution of living  
995 planktonic foraminifera from the Panama Basin. *Nature* 298, 841-844.

996 Ferretti, P., Crowhurst, S.J., Naafs, B.D.A., Barbante, C., 2015. The Marine Isotope Stage 19 in the mid-  
997 latitude North Atlantic Ocean: astronomical signature and intra-interglacial variability: Quaternary  
998 Science Reviews 108, 95-110.

999 Fletcher, C.G., Kushner, P.J., Hall, A., Quet, X., 2009. Circulation responses to snow albedo feedback in  
1000 climate change. *Geophysical Research Letters* 36, L09702, doi:10.1029/2009GL038011.

1001 Flores, J.A., Sierro, F.J., 1997. Revised technique for calculation of calcareous nannofossil accumulation  
1002 rates. *Micropaleontology* 43, 321-324.

1003 Fraile, I., Schulz, M., Mulitza, S., Kucera, M., 2008. Predicting the global distribution of planktonic  
1004 foraminifera using a dynamic ecosystem model. *Biogeosciences* 5, 891-911.

1005 Frigola, J., Moreno, A., Cacho, I., Canals, M., Sierro, F. J., Flores, J. A., Grimalt, J. O., (2008), Evidence of  
1006 abrupt changes in Western Mediterranean Deep Water circulation during the last 50 kyr: A high-  
1007 resolution marine record from the Balearic Sea, *Quat. Int.* 181, 88-104,  
1008 doi:10.1016/j.quaint.2007.1006.1016



- 1009 Frisia, S., Borsato, A., Spötl, C., Villa, I.M., Cucchi, F., 2005. Climate variability in the SE alps of Italy over  
1010 the past 17 000 years reconstructed from a stalagmite record. *Boreas* 34 (4), 445-455.
- 1011 Gačić, M., Eusebi Borzelli, G. L., Civitarese, G., Cardin, V., Yari, S., 2010, Can internal processes sustain  
1012 reversals of the ocean upper circulation? The Ionian Sea example. *Gophysical Research Letters* 37,  
1013 L09608, doi:10.1029/2010GL043216,
- 1014 Ganopolski, A., Rahmstorf, S., 2001. Rapid changes of glacial climate simulated in a coupled model. *Nature*  
1015 409, 153-158.
- 1016 Geisen, M., Billard, C., Broerse, A.T.C., Cros, L., Probert, I., Young, J.R., 2002. Life-cycle associations  
1017 involving pairs of holococcolithophorid species: intraspecific variation or cryptic speciation? *Eur. J.*  
1018 *Phycol.* 37, 531-550.
- 1019 Geraga, M., Tsaila-Monopolis, S., Ioakim, C., Papatheodorou, G., Ferentinos, G., 2000, Evaluation of  
1020 palaeoenvironmental changes during the last 18,000 years in the Myrtoon basin, SW Aegean Sea,  
1021 *Palaeogeogr. Palaeoclimatol. Palaeoecol.* 156, 1-17.
- 1022 Geraga, M., Tsaila-Monopolis, S., Ioakim, C., Papatheodorou, G., Ferentinos, G., 2005. Shortterm climate  
1023 changes in the southern Aegean Sea over the last 48,000 years. *Palaeogeography Palaeoclimatology*  
1024 *Palaeoecology* 220, 311-332.
- 1025 Geraga, M., Mylona, G., Tsaila-Monopolis, S., Papatheodorou, G., Ferentinos, G., 2008. Northeastern Ionian  
1026 Sea: palaeoceanographic variability over the last 22 ka. *J. Mar. Syst.* 74, 623-638.
- 1027 Giaccio, B., Regattieri, E., Zanchetta, G., Nomade, S., Renne, P.R., Sprain, C.J, Drysdale, R.N., Tzedakis,  
1028 P.C., Messina, P., Scardia, G., Sposato, A., Bassinot, F., 2015. Duration and dynamics of the best orbital  
1029 analogue to the present interglacial. *Geology*, doi:10.1130/G36677.1
- 1030 Giraudi, C., Magny, M., Zanchetta, G., Drysdale, R.N., 2011. The Holocene climatic evolution of  
1031 Mediterranean Italy: a review of the continental geological data. *The Holocene* 21 (1), 105-115.
- 1032 Girone, A., 2005, Response of otolith assemblages to sea-level fluctuations at the Lower Pleistocene  
1033 Montalbano Jonico section (southern Italy): *Bollettino della Società Paleontologica Italiana* 44 (1), 35-45.
- 1034 Girone, A., Capotondi, L., Ciaranfi, N., Di Leo, P., Lirer, F., Maiorano, P., Marino, M., Pelosi, N., Pulice, I.,  
1035 2013. Paleoenvironmental change at the lower Pleistocene Montalbano Jonico section (southern Italy):  
1036 global versus regional signals: *Palaeogeography, Palaeoclimatology, Palaeoecology* 371, 62-79.
- 1037 Giunta, S., Negri, A., Maffioli, P., Sangiorgi, F., Capotondi, L., Morigi, C., Principato, M.S., Corselli, C.,  
1038 2006. Phytoplankton dynamics in the eastern Mediterranean Sea during marine isotopic stage 5e.  
1039 *Palaeogeogr. Palaeoclimatol. Palaeoecol.* 235, 28-47.
- 1040 Goudeau, M.-L.S., Grauel, A.L., Bernasconi, S.M., de Lange, G.J., 2013. Provenance of surface sediments  
1041 along the southeastern Adriatic coast off Italy: an overview. *Estuar. Coast. Shelf Sci.* 134, 45-56.
- 1042 Goudeau, M.-L.S., Grauel, A.L., Tessarolo, C., Leider, A., Chen, L., Bernasconi, S.M., Versteegh, G. J.M.,  
1043 Zonneveld, K.A.F., Boer, W., Alonso-Hernandez, C.M., De Lange, G.J., 2014. The Glacial–Interglacial  
1044 transition and Holocene environmental changes in sediments from the Gulf of Taranto, Central  
1045 Mediterranean. *Mar. Geol.* 348, 88-102.
- 1046 Gran, H.H., Braarud, T., 1935: A quantitative study of the phytoplankton in the Bay of Fundy and the Gulf  
1047 of Maine (including observations on hydrography, chemistry and turbidity). *Biological Board of Canada,*  
1048 *Journal* 1, no. 5, 279-467.
- 1049 Grauel, A.L., Bernasconi, S.M., 2010. Core-top calibration of  $\delta^{18}\text{O}$  and  $\delta^{13}\text{C}$  of *G. ruber* (white) and *U.*  
1050 *mediterranea* along the southern Adriatic coast of Italy. *Mar. Micropaleontol.* 77 (3-4), 175-186 (12).
- 1051 Grauel, A.L., Goudeau, M.L.S., de Lange, G.J., et al., 2013. Climate of the past 2500 years in the Gulf of  
1052 Taranto, central Mediterranean Sea: a high-resolution climate reconstruction based on  $\delta^{18}\text{O}$  and  $\delta^{13}\text{C}$  of  
1053 *Globigerinoides ruber* (white). *The Holocene* 23, 1440–1446.
- 1054 Hayes, A., Rohling, E.J., De Rijk, S., Kroon, D., Zachariasse, W.J., 1999. Mediterranean planktonic  
1055 foraminiferal faunas during the last glacial cycle. *Mar. Geol.* 153, 239–252.
- 1056 Hayes, A., Kucera, M., Kallel, N., Saffi, L., Rohling, E.J., 2005. Glacial Mediterranean sea surface  
1057 temperatures reconstructed from planktonic foraminiferal assemblages. *Quat. Sci. Rev.* 24, 999-1016.
- 1058 Head, M., 2019. Formal subdivision of the Quaternary System/Period: Present status and future directions.  
1059 *Quaternary Intern.* <https://doi.org/10.1016/j.quaint.2019.05.018>.
- 1060 Hemleben, C., Spindler, M., Anderson, O.R., 1989. *Modern Planktonic Foraminifera*. Springer-Verlag, New  
1061 York, 363 pp.

1062 Herbert, T., 2003, Alkenone paleotemperature determinations. In: Treatise on geochemistry, Ed. Elderfield,  
1063 H. Executive Editors: Holland, H.D., Turekian, K.K., 391-432pp. ISBN 0-08-043751-6. Elsevier, 2003.

1064 Hodell, D.A., Crowhurst, S., Skinner, L., Tzedakis, P.C., Margari, V., Channell, J.E.T., Kamenov, G.,  
1065 Maclachlan, S., Rothwell, G., 2013. Response of Iberian Margin sediments to orbital and suborbital  
1066 forcing over the past 420 ka. *Paleoceanography* 28. <http://dx.doi.org/10.1002/palo.20017>.

1067 Hodell, D., Lourens, L., Crowhurst, S., Konijnendijk, T., Tjallingii, R., Jimenez- Espejo, F., Skinner, L.,  
1068 Tzedakis, P.C., Shackleton Site Project Members, 2015. A reference time scale for site U1385  
1069 (Shackleton site) on the SW Iberian margin. *Global Planet. Change* 133, 48-64.

1070 Hurrell, J.W., Hoerling, M.P., Phillips, A., Xu, T., 2004. Twentieth century north Atlantic climate change.  
1071 Part I: assessing determinism. *Clim Dyn* 23, 371-389.

1072 Incarbona, A., Sprovieri, M., Di Stefano, A., Di Stefano, E., Salvagio Manta, D., Pelosi, N., Ribera d'Alcalà,  
1073 M., Sprovieri, R., Ziveri, P., 2013. Productivity modes in the Mediterranean Sea during Dansgaard–  
1074 Oeschger (20,000–70,000 yr ago) oscillations. *Palaeogeography, Palaeoclimatology, Palaeoecology* 392,  
1075 128-137.

1076 Johannessen, T., Jansen, E., Flatoy, A., Ravelo, A.C., 1994. The relationship between surface water masses,  
1077 oceanographic fronts and paleoclimatic proxies in surface sediments of the Greenland, Iceland and  
1078 Norwegian seas. In: Zahn, R., Pedersen, T.F., Kaminski, M.A., Labeyrie, L. (Eds.), *Carbon Cycling in the  
1079 Glacial Ocean: Constraints on the Ocean's Role in Global Change*. NATO Asi Series, I, 17. Springer,  
1080 Heidelberg, pp. 61–86.

1081 Kwiecien, O., Arz, H.W., Lamy, F., Plessen, B., Bahr, A., Haug, G.H., 2009. North Atlantic control on  
1082 precipitation pattern in the eastern Mediterranean/Black Sea region during the last glacial. *Quaternary  
1083 Research* 71, 375-384

1084 Kleiven, H., Hall, I.R., McCave, I.N., Knorr, G., Jansen, E., 2011. North Atlantic coupled deep-water flow  
1085 and climate variability in the middle Pleistocene: *Geology* 39 (4), 343-346.

1086 Konijnendijk, T.Y.M., Ziegler, M., Lourens, L.J., 2014, Chronological constraints on Pleistocene sapropel  
1087 depositions from high-resolution geochemical records of ODP Sites 967 and 968: *Newsletters on  
1088 Stratigraphy* 47 (3), 263-282.

1089 Kontiokis, G., 2016. Late Quaternary paleoenvironmental reconstruction and paleoclimatic implications of  
1090 the Aegean Sea (eastern Mediterranean) based on paleoceanographic indexes and stable isotopes.  
1091 *Quaternary International* 401, 28-42.

1092 Laskar, J., Robutel, P., Joutel, F., Gastineau, M., Correia, A.C.M., and Levrard, B., 2004. A long  
1093 term numerical solution for the insolation quantities of the Earth: *Astronomy & Astrophysics* 428, 261-  
1094 285, <http://dx.doi.org/10.1051/0004-6361:20041335>.

1095 Leaman, K.D., Schott, F.A., 1991. Hydrographic structure of the convection regime in the Gulf of Lions:  
1096 winter 1987. *Journal of Physical Oceanography* 21, 575-598.

1097 Lirer, F., Sprovieri, M., Ferraro, L., Vallefucio, M., Capotondi, L., Cascella, A., Petrosino, P., Insinga, D.D.,  
1098 Pelosi, N., Tamburrino, S., Lubritto, C., 2013. Integrated stratigraphy for the late Quaternary in the  
1099 eastern Tyrrhenian sea. *Quat. Int.* 292, 71–85.

1100 Lisiecki, L.E., Raymo, M.E., 2005. A Pliocene-Pleistocene stack of 57 globally distributed benthic  $\delta^{18}\text{O}$   
1101 records: *Paleoceanography* 20, PA1003.

1102 Locarnini, R. A., Mishonov, A. V., Antonov, J. I., Boyer, T. P., Garcia, H. E., 2010, *World Ocean Atlas  
1103 2009. Volume 1: Temperature*; NOAA Atlas NESDIS 68, NOAA, U.S. Government Printing Office,  
1104 Washington D.C.

1105 Lourens, L.J., 2004. Revised tuning of Ocean Drilling Program Site 964 and KC01B (Mediterranean) and  
1106 implications for the  $\delta^{18}\text{O}$ , tephra, calcareous nannofossil, and geomagnetic reversal chronologies of the  
1107 past 1.1 Myr: *Paleoceanography* 19, PA3010.

1108 Lourens, L., Hilgen, F., Shackleton, N.J., Laskar, J., Wilson, D., 2004. The Neogene period: in Gradstein,  
1109 F.M., Ogg, J.G., Smith, A.G. (Eds.), *A Geological Time Scale*. Cambridge University Press, pp. 409-440.

1110 Maheras, P., Xoplaki, E., Kutiel, H., 1999. Wet and dry monthly anomalies across the Mediterranean basin  
1111 and their relationship with circulation 1860–1990, *Theor. Appl. Climatol.* 64, 189-199,

1112 Maiorano, P., Marino, M., Di Stefano, E., Ciaranfi, N., 2004, Calcareous nannofossil events in the lower-  
1113 middle Pleistocene transition at the Montalbano Jonico section and ODP Site 964: calibration with  
1114 isotope and sapropel stratigraphy: *Rivista Italiana di Paleontologia e Stratigrafia* 110, 547-557.

- 1115 Maiorano, P., Aiello, G., Barra, D., Di Leo, P., Joannin, S., Lirer, F., Marino, M., Pappalardo, A., Capotondi,  
 1116 L., Ciaranfi, N., Stefanelli, S., 2008. Paleoenvironmental changes during sapropel 19 (i-cycle 90)  
 1117 deposition: evidences from geochemical, mineralogical and microplaoentological proxies in the mid  
 1118 Pleistocene Montalbano Jonico land section (southern Italy): Palaeogeography, Palaeoclimatology,  
 1119 Palaeoecology 257, 308-334.
- 1120 Maiorano, P., Capotondi, L., Ciaranfi, N., Girone, A., Lirer, F., Marino, M., Pelosi, N., Petrosino, P.,  
 1121 Piscitelli, A., 2010. Vrica-Crotone and Montalbano Jonico sections: a potential unit-stratotype of the  
 1122 Calabrian Stage. Episodes 33, 218-233.
- 1123 Maiorano, P., Tarantino, F., Marino, M., De Lange, G.J., 2013. Paleoenvironmental conditions at Core  
 1124 KC01B (Ionian Sea) through MIS 13-9: evidence from calcareous nannofossil assemblages. Quat. Int.  
 1125 288, 97-111.
- 1126 Maiorano, P., Marino, M., Balestra, B., Flores, J.A., Hodell, D.A., Rodrigues, T., 2015. Coccolithophore  
 1127 variability from the Shackleton Site (IODP Site U1385) through MIS 16–10. Glob. Planet. Change 133,  
 1128 35-48.
- 1129 Maiorano, P., Bertini, A., Capolongo, D., Eramo, G., Gallicchio, S., Girone, A., Pinto, D., Toti, F., Ventrucci,  
 1130 G., Marino, M., 2016a. Climate signatures through the Marine Isotope Stage 19 in the Montalbano Jonico  
 1131 section (Southern Italy): a land-sea perspective: Palaeogeography, Palaeoclimatology, Palaeoecology 461,  
 1132 341-361.
- 1133 Maiorano, P., Girone, A., Marino, M., Kucera, M., Pelosi, N., 2016b. Sea surface water variability during the  
 1134 Mid-Brunhes inferred from calcareous plankton in the western Mediterranean (ODP Site 975).  
 1135 Palaeogeography, Palaeoclimatology, Palaeoecology 459, 229-248.
- 1136 Malanotte-Rizzoli, P., Manca, B. B., Ribera d'Alcala, M., Theocharis, A., Brenner, S., Budillon, G., Ozsoy,  
 1137 E., 1999. The eastern Mediterranean in the 80s and in the 90s: The big transition in the intermediate and  
 1138 deep circulations, Dyn. Atmos. Oceans 29, 365- 395.
- 1139 Malanotte-Rizzoli, P., Artale, V., Borzelli-Eusebi, G.L., Brenner, S., Crise, A., Gacic, M., Kress, N.,  
 1140 Marullo, S., Ribera d'Alcalà, M., Sofianos, S., Tanhua, T., Theocharis, A., Alvarez, M., Ashkenazy, Y.,  
 1141 Bergamasco, A., Cardin, V., Carniel, S., Civitarese, G., D'Ortenzio, F., Font, J., Garcia-Ladona, E.,  
 1142 Garcia-Lafuente, J.M., Gogou, A., Gregoire, M., Hainbucher ,D., Kontoyannis, H., Kovacevic ,V.,  
 1143 Kraskapoulou, E., Kroskos ,G., Incarbona, A., Mazzocchi, M.G., Orlic, M., Ozsoy, E., Pascual, A.,  
 1144 Poulain, P.M., Roethe, W., Rubino, A., Schroeder, K., Siokou-Frangou, J., Souvermezoglou, E.,  
 1145 Sprovieri, M., Tintoré, J., Triantafyllou, G., 2014. Physical forcing and physical/biochemical variability  
 1146 of the Mediterranean Sea: a review of unresolved issues and directions for future research. Ocean Science  
 1147 10, 281-322.
- 1148 Mallo, M., Ziveri, P., Mortyn, P.G., Schiebel, R., Grelaud, M., 2017. Low planktic foraminiferal diversity  
 1149 and abundance observed in a spring 2013 west–east Mediterranean Sea plankton tow transect.  
 1150 Biogeosciences 14, 2245-2266.
- 1151 Marino, M., Maiorano, P., Flower, B.P., 2011. Calcareous nannofossil changes during the Mid- Pleistocene  
 1152 revolution: paleoecologic and paleoceanographic evidence from North Atlantic Site 980/981.  
 1153 Palaeogeogr. Palaeoclimatol. Palaeoecol. 306 (1-2), 58-69.
- 1154 Marino, M., Maiorano, P., Tarantino, F., Voelker, A., Capotondi, L., Girone, A., Lirer, F., Flores, J.-A.,  
 1155 Naafs, B.D.A., 2014. Coccolithophores as proxy of seawater changes at orbital- to-millennial scale during  
 1156 middle Pleistocene Marine Isotope Stages 14–9 in North Atlantic core MD01-2446. Paleoceanography  
 1157 29. <http://dx.doi.org/10.1002/2013PA002574>.
- 1158 Marino, M., Bertini, A., Ciaranfi, N., Aiello, G., Barra, D., Gallicchio, S., Girone, A., La Perna, R., Lirer, F.,  
 1159 Maiorano, P., Petrosino, P., Toti, F., 2015. Paleoenvironmental and climatostratigraphic insights for  
 1160 Marine Isotope Stage 19 (Pleistocene) at the Montalbano Jonico section, South Italy: Quaternary  
 1161 International 383, 104-115. <http://dx.doi.org/10.1016/j.quaint.2015.01.043>.
- 1162 Marino, M., Aiello, G., Barra, D., Bertini, A., Gallicchio, S., Girone, A., La Perna, R., Lirer, F., Maiorano,  
 1163 P., Petrosino, P., Quivelli, O., Toti, F., Ciaranfi, N., 2016. The Montalbano Jonico section (South Italy) as  
 1164 a reference for the Early/Middle Pleistocene boundary. Alpine and Mediterranean Quaternary 29 (1), 45-  
 1165 57.
- 1166 Marino, M., Girone, A., Maiorano, P., Di Renzo, R., Piscitelli, A., Flores, J.-A., 2018. Calcareous plankton  
 1167 and the mid-Brunhes climate variability in the Alboran Sea (ODP Site 977). Palaeogeography,  
 1168 Palaeoclimatology, Palaeoecology 508, 91-106.

1169 Mariolopoulos, E.G., 1961. An outline of the climate of Greece, Publications of the Meteorological Institute  
1170 of the University of Athens 6, 51 pp.

1171 Martin-Garcia, G.M., Sierro, F.J., Flores J.-A., Abrantes, F., 2018. Change in the North Atlantic circulation  
1172 associated with the mid-Pleistocene transition. *Clim. Past*, 14, 1639–1651. [https://doi.org/10.5194/cp-14-](https://doi.org/10.5194/cp-14-1639-2018)  
1173 1639-2018.

1174 Martinez, J.I., Mora, G., Barrows, T.T., 2007. Paleoceanographic conditions in the western Caribbean Sea  
1175 for the last 560 kyr as inferred from planktonic foraminifera. *Marine Micropaleontology* 64, 177-188.

1176 Martrat, B., Jimenez-Amat, P., Zahn, R., Grimalt, J.O., 2014. Similarities and dissimilarities between the last  
1177 two deglaciations and interglaciations in the North Atlantic region. *Quaternary Science Reviews* 99, 112-  
1178 134.

1179 Maselli, V., Hutton, E.W., Kettner, A.J., Syvtski, J.P.M., Trincardi, F., 2011. High-frequency sea level and  
1180 sediment supply fluctuations during Termination I: An integrated sequence-stratigraphy and modeling  
1181 approach from the Adriatic Sea (Central Mediterranean). *Marine Geology* 287, 54-70 pp.

1182 McIntyre, A., Bé, A.H.W., 1967. Modern coccolithophores of the Atlantic Ocean - I. Placolith and cyrtoliths.  
1183 *Deep Sea Res.* 14, 561-597.

1184 Melki, T., Kallel, N., Jorissen, F.J., Guichard, F., Dennielou, B., Berné, S., Labeyrie, L., Fontugne, M., 2009.  
1185 Abrupt climate change, sea surface salinity and paleoproductivity in the western Mediterranean Sea (Gulf  
1186 of Lion) during the last 28 kyr. *Palaeogeogr. Palaeoclimatol. Palaeoecol.* 279 (96-111).

1187 Miller, K.G., Wright, J.D., 2017. Success and failure in Cenozoic global correlations using golden spikes: A  
1188 geochemical and magnetostratigraphic perspective. *Episodes* 40 (1), 1-22.

1189 Milligan, T.G., Cattaneo, A., 2007. Sediment Dynamics in the Western Adriatic Sea: From transport to  
1190 stratigraphy. *Continental Shelf Research* 27, 287-295

1191 Molfino, B., McIntyre, A., 1990. Nutricline variation in the equatorial Atlantic coincident with the Younger  
1192 Dryas. *Paleoceanography* 5, 997-1008.

1193 Morard, R., Quillévéré, F., Escarguel, G., Ujiie, Y., de Garidel-Thoron, T., Norris, R.D., de Vargas, C., 2009.  
1194 Morphological recognition of cryptic species in the planktonic foraminifer *Orbulina universa*. *Mar.*  
1195 *Micropaleontol.* 71, 148-165.

1196 Moreno, A., Cacho, I., Canals, M., Prins, M. A., Sánchez-Goñi, M. F., Grimalt, J. O., Weltje, G. J., 2002.  
1197 Saharan dust transport and high-latitude glacial climatic variability: the Alboran Sea record. *Quaternary*  
1198 *Research* 58(3), 318-328.

1199 Moreno, A., Cacho, I., Canals, M., Grimalt, J. O., Sanchez-Vidal, A., 2004. Millennial-scale variability in  
1200 the productivity signal from the Alboran Sea record, Western Mediterranean Sea. *Palaeogeography,*  
1201 *Palaeoclimatology, Palaeoecology* 211(3-4), 205-219.

1202 Moreno, A., Cacho, I., Canals, M., Grimalt, J. O., Sánchez-Goñi, M. F., Shackleton, N., Sierro, F. J., 2005.  
1203 Links between marine and atmospheric processes oscillating on a millennial time-scale. A multi-proxy  
1204 study of the last 50,000 yr from the Alboran Sea (Western Mediterranean Sea). *Quaternary Science*  
1205 *Reviews* 24(14-15), 1623-1636.

1206 Moscariello, A., Ravazzi, C., Brauer, A., Mangili, C., Chiesa, S., Rossi, S., de Beaulieu, J.L., Reille, M.,  
1207 2000. A long lacustrine record from the Pianico-Sellere basin (Middle-Late Pleistocene, Northern Italy).  
1208 *Quat. Int.* 73-74, 47-68.

1209 Müller, P.J., Kirst, G., Ruhland, G., von Storch, I., Rosel-Melé, A., 1998. Calibration of the alkenone  
1210 paleotemperature index  $U_{37}^{K'}$  based on core-tops from the eastern North Atlantic and the global ocean  
1211 (60N-60S). *Geochimica et Cosmochimica Acta* 62, 1757-1772.

1212 Narciso, A., Flores, J.-A., Cachão, M., Sierro, F.-J., Colmenero-Hidalgo, E., Piva, A., Asioli, A., 2010. Sea  
1213 surface dynamics and coccolithophore behaviour during sapropel deposition of Marine Isotope Stage 7, 6  
1214 and 5 in the Western Adriatic Sea. *Revista Española de Micropaleontología* 42, 345-358.

1215 Naughton, F., Drago, T., Sánchez Goñi, M.F., Freitas, M.C., 2011. Climate variability in the North-Western  
1216 Iberian Peninsula during the last deglaciation. In: *Oceans and the Atmospheric Carbon Content*. Springer,  
1217 Netherlands, pp. 1-22.

1218 Naughton, F., Sánchez Goñi, M.F., Rodrigues, T., Salueiro, E., Costas, S., Desprat, S., Duprat, J., Michel,  
1219 E., Rossignol, L., Zaragosi, S., Voelker, A.H.L., Abrantes, F., 2016. Climate variability across the last  
1220 deglaciation in NW Iberia and its margin. *Quat. Int.* 414, 9–22.

1221 North Greenland Ice Core Project members. 2004. High-resolution record of Northern Hemisphere climate  
1222 extending into the last interglacial period. *Nature*, 431, pp. 147-151.

- 1223 Nomade, S., Bassinot, F., Marino, M., Simon, Q., Dewilde F., Maiorano, P., Esguder, G., Blamart, D.,  
 1224 Girone, A., Scao, V., Pereira, A., Toti, F., Bertini, A., Combourieu-Nebout, N., Peral, M., Bourles, D.,  
 1225 Petrosino, P., Gallicchio, S., Ciaranfi, N., 2019. High-resolution foraminifer stable isotope record of MIS  
 1226 19 at Montalbano Jonico, southern Italy: a window into Mediterranean climatic variability during a low-  
 1227 eccentricity interglacial. *Quaternary Science Reviews* 205, 106-125.
- 1228 Palumbo, E., Flores, J.A., Perugia, C., Petrillo, Z., Voelker, A.H.L., Amore, F.O., 2013. Millennial-scale  
 1229 coccolithophore paleoproductivity and surface water changes between 445 and 360 ka (Marine Isotope  
 1230 Stages 12/11) in the Northeast Atlantic. *Palaeogeogr. Palaeoclimatol. Palaeoecol.* 383-384, 27-41.
- 1231 Parente, A., Cachão, M., Baumann, K.-H., de Abreu, L., Ferreira, J., 2004. Morphometry of *Coccolithus*  
 1232 *pelagicus* s.l. (Coccolithophore, Haptophyta) from offshore Portugal, during the last 200 kyr.  
 1233 *Micropaleontology* 50, 107-120.
- 1234 Patacca, E., Scandone, P., 2007, *Geology of the Southern Apennines: Bollettino della Società Geologica*  
 1235 *Italiana, Special Issue, v. 7, pp. 75-119.*
- 1236 Paterne, M., Nejib, K., Labeyrie, L.D., Vautravers, M. Duplessy J.C., Rossignol-Strick, M., Cortijo,  
 1237 E., Arnold, M., Fontugne, M., R., 1999. Hydrological relationship between the North Atlantic  
 1238 Ocean and the Mediterranean Sea during the past 15-75 kyr. *Paleoceanography*, 14 (5), 626-638.
- 1239 Peral, M., Blamart, D., Bassinot, F., Daëron, M., Dewilde, F., Rebaubier, H., Nomade, S., Girone, A.,  
 1240 Marino, M., Maiorano, P., Ciaranfi, N., 2020. Changes in temperature and oxygen isotopic composition  
 1241 of Mediterranean water during the Mid-Pleistocene transition in the Montalbano Jonico section (southern  
 1242 Italy) using the clumped-isotope thermometer. *Palaeogeography, Palaeoclimatology, Palaeoecology*, 544,  
 1243 109603. <https://doi.org/10.1016/j.palaeo.2020.109603>.
- 1244 Pérez-Folgado, M., Sierro, F.J., Flores, J.A., Cacho, I., Grimalt, J.O., Zahn, R., Shackleton, N., 2003.  
 1245 Western Mediterranean planktonic foraminifera events and millennial climatic variability during the last  
 1246 70 kyr. *Mar. Micropaleontol.* 48, 49-70.
- 1247 Pescatore, T., Pieri, P., Sabato, L., Senatore, M.R., Gallicchio, S., Boscaino, M., Cilumbriello, A.,  
 1248 Quarantiello, R., Capretto, G., 2009. Stratigrafia dei depositi pleistocenico-olocenici dell'area costiera di  
 1249 Metaponto compresa fra Marina di Ginosa ed il Torrente Cavone (Italia meridionale): Carta Geologica in  
 1250 scala 1:25.000. *Il Quaternario* 22 (2), 307-323.
- 1251 Petrosino, P., Jicha, B.R., Mazzeo, F.C., Ciaranfi, N., Girone, A., Maiorano, P., Marino, M., 2015. The  
 1252 Montalbano Jonico marine succession: An archive for distal tephra layers at the Early-Middle Pleistocene  
 1253 boundary in southern Italy: *Quaternary International* 383, 89-103,  
 1254 <http://dx.doi.org/10.1016/j.quaint.2014.10.049>.
- 1255 Pinardi, N., Masetti, E., 2000. Variability of the large scale general circulation of the mediterranean sea from  
 1256 observations and modelling: a review. *Palaeogeography, Palaeoclimatology, Palaeoecology* 158 (2000)  
 1257 153173 (2000).
- 1258 Piva, A., Asioli, A., Trincardi, F., Schneider, R.R., Vigliotti, L., 2008. Late-Holocene climate variability in  
 1259 the Adriatic Sea (Central Mediterranean). *The Holocene* 18 (1), 153-167.
- 1260 Pol, K., Masson-Delmotte, V., Johnsen, S., Bigler, M., Cattani, O., Durand, G., Falourd, S., Jouzel, J.,  
 1261 Minster, B., Parrenin, F., Ritz, C., Steen-Larsen, H. C., Stenni, B., 2010. New MIS 19 EPICA Dome C  
 1262 high-resolution deuterium data: hints for a problematic preservation of climate variability in the “oldest  
 1263 ice”: *Earth and Planetary Science Letters* 298, (1-2), 95-103, doi:10.1016/j.epsl.2010.07.030, 2010.
- 1264 Poulain, P.-M., 2001. Adriatic Sea surface circulation as derived from drifter data between 1990 and 1999, *J.*  
 1265 *Marine Syst.* 29, 3-32.
- 1266 Poulain, P.-M., Menna, M., Mauri, E., 2012. Surface geostrophic circulation of the Mediterranean Sea  
 1267 derived from drifter and satellite altimeter data, *J. Phys. Ocean.* doi:http://dx.doi.org/10.1175/JPO-D-11-  
 1268 0159.1
- 1269 Poulos, S.E., Drakopoulos, P.G., Collins, M.B., 1997. Seasonal variability in sea surface oceanographic  
 1270 conditions in the Aegean Sea (Eastern Mediterranean): an overview. *Journal of Marine Systems* 13, 225-  
 1271 244.
- 1272 Pros, J., Kotthoff, U., Müller, U.C., Peyron, O., Dormoy, I., Schmiedl, G., Kalaitzidis, S., Smith, A.M., 2009.  
 1273 Massive perturbation in terrestrial ecosystems of the Eastern Mediterranean region associated with the 8.2  
 1274 kyr B.P. climatic event. *Geology* 37(10), 887-890. doi: 10.1130/G25739A.1.

- 1275 Pujol, C., Vergnaud-Grazzini, C., 1995. Distribution patterns of live planktic foraminifers as related to  
1276 regional hydrography and productive systems of the Mediterranean Sea. *Mar. Micropaleontol.* 25, 187-  
1277 217.
- 1278 Quivelli, O., 2020. Coccolithophores and biomarkers as paleoclimatic and paleoceanographic indicators  
1279 during Marine Isotope Stage 2015. PhD Thesis, 189 pp. Università degli studi di Bari Aldo Moro. Bari,  
1280 Italy.
- 1281 Quivelli, O., Marino, M., Rodrigues, T., Girone, A., Maiorano, P., Abrantes, F., Salgueiro, E., Bassinot, F.,  
1282 2020. Surface and deep water variability in the Western Mediterranean (ODP Site 975) during insolation  
1283 cycle 74: High-resolution calcareous plankton and molecular biomarker signals. *Palaeogeography,*  
1284 *Palaeoclimatology, Palaeoecology* 542,109583. <https://doi.org/10.1016/j.palaeo.2019.109583>.
- 1285 Railsback, L.C., Gibbard, P.L., Heas, M.J., Voarintsoa, N.R.G., Tucanne, S., 2015. An optimized scheme of  
1286 lettered marine isotope substages for the last 1.0 million years, and the climatostratigraphic nature of  
1287 isotope stages and substages. *Quat. Sci. Rev.* 111, 94-106.
- 1288 Raymo, M.E., Ruddiman, W.F., Rind, D., 1990. Climatic effects of reduced Arctic sea ice limits in the GISS-  
1289 II GCM. *Paleoceanography* 5, 367-382.
- 1290 Raymo, M.E., Oppo, D.W., Curry, W., 1997. The mid-Pleistocene climate transition: a deep-sea carbon  
1291 isotopic perspective. *Paleoceanography* 12, 546-559
- 1292 Reynolds, L.A., Thunell, R.C., 1986. Seasonal production and morphologic variation of *Neogloboquadrina*  
1293 *pachyderma* (Ehrenberg) in the northeast Pacific, *Micropaleontology* 32, 1-18.
- 1294 Repschläger, J., Weinelt, M., Kinkel, H., Andersen, N., GarbeSchönberg, D., Schwab, C., 2015. Response of  
1295 the subtropical North Atlantic surface hydrography on deglacial and Holocene AMOC changes,  
1296 *Paleoceanography* 30, 456-476, doi:10.1002/2014pa002637.
- 1297 Regattieri, E., Giaccio, B., Mannella, G., Zanchetta, G., Nomade, S., Tognarelli, A., Perchiazzi, N., Vogel,  
1298 H., Boschi, C., Neil, R. D., Wagner, B., Gemelli, M., Tzedakis, P., 2019. Frequency and dynamics of  
1299 millennial-scale variability during Marine Isotope Stage 19: Insights from the Sulmona Basin (central  
1300 Italy). *Quaternary Science Reviews* 214, 28-43
- 1301 Rio, D., Raffi, I., and Villa, G., 1990, Pliocene-Pleistocene distribution patterns in the Western  
1302 Mediterranean: in Karstetn, K.A., Mascle, J., et al. (Eds.), *Proceedings of ODP, Scientific Results* 107,  
1303 513-533.
- 1304 Roberts, N., Jones, M.D., Benkaddur, A., Eastwood, W.J., Filippi, M.L., Frogley, M.R., Lamb, H.F., Leng,  
1305 M.J., Reed, J.M., Stein, M., Stevens, L., Valero-Garces, B., Zanchetta, G., 2008. Stable isotope records of  
1306 Late Quaternary climate and hydrology from Mediterranean lakes: the ISOMED synthesis. *Quat. Sci.*  
1307 *Rev.* 27, 2426-2441.
- 1308 Rodrigo-Gámiz, M., Martínez-Ruiz, F., Jiménez-Espejo, F. J., Gallego-Torres, D., Nieto-Moreno, V.,  
1309 Romero, O., Ariztegui, D., 2011. Impact of climate variability in the western Mediterranean during the  
1310 last 20,000 years: oceanic and atmospheric responses. *Quaternary Science Reviews* 30(15), 2018-2034.
- 1311 Rodrigues, T., Voelker, A.H.L., Grimalt, J.O., Abrantes, F., Naughton, F., 2011. Iberian margin sea surface  
1312 temperature during MIS 15 to 9 (580–300 ka): glacial suborbital variability versus interglacial stability.  
1313 *Paleoceanography* 26, PA1204. <https://doi.org/10.1029/2010PA001927>.
- 1314 Rodrigues, T., Alonso-García, M., Hodell, D.A., Rufino, M., Naughton, F., Grimalt, J.O., Voelker, A.H.L.,  
1315 Abrantes, F., 2017. A 1-Ma record of sea surface temperature and extreme cooling events in the North  
1316 Atlantic: a perspective from the Iberian margin. *Quat. Sci. Rev.* 172, 118-130.
- 1317 Rogerson, M., Cacho, I., Jimenez-Espejo, F., Reguera, M.I., Sierro, F.J., Martinez-Ruiz, F., Frigola, J.,  
1318 Canals, M., 2008. A dynamic explanation for the origin of the western Mediterranean organic rich layers.  
1319 *Geochem. Geophys. Geosyst.* 9, Q07U01. <https://doi.org/10.1029/2007GC001936>.
- 1320 Rohling, E.J., Gieskes, W.W.C., 1989. Late Quaternary changes in Mediterranean intermediate water density  
1321 and formation rate. *Paleoceanography* 4, 531–545.
- 1322 Rohling, E.J., Jorissen, F.J., Vergnaud Grazzini, C., Zachariasse, W.J., 1993. Northern Levantine and  
1323 Adriatic Quaternary planktic foraminifera; reconstruction of paleoenvironmental gradients. *Mar.*  
1324 *Micropaleontology* 21, 191-218
- 1325 Rohling, E.J., den Dulk, M., Pujol, C., Vergnaud-Grazzini, C., 1995. Abrupt hydrographic changes in the  
1326 Alboran Sea (western Mediterranean) around 8000 yrs BP. *Deep-Sea Res.* 42, 1609-1619

- 1327 Rohling, E.J., Jorissen, F.J., De Stigter, H.C., 1997. 200-year interruption of Holocene sapropel formation in  
1328 the Adriatic Sea. *J. Micropalaeontol.* 16 (2), 97-108.
- 1329 Rohling, E.J., Hayes, A., De Rijk, S., Kroon, D., Zachariasse, W.J., Eisma, D., 1998. Abrupt cold spells in  
1330 the Northwest Mediterranean. *Paleoceanography* 13, 316-322.
- 1331 Rohling, E.J., Mayewski, P.A., Hayes, A., Abu-Zied, R.H., Casford, J.S.L., 2002. Holocene atmosphere-  
1332 ocean interactions: records from Greenland and the Aegean Sea. *Clim. Dyn.* 18, 587-593.
- 1333 Rohling, E.J., Hayes, A., Mayewski, P.A.; Kucera, M., 2009. Holocene climate variability in the eastern  
1334 Mediterranean, and the End of the Bronze Age. In: Bachhuber, C., Roberts, G. (Eds.), *Forces of*  
1335 *Transformation: The End of the Bronze Age in the Mediterranean.* Oxbow Books, Oxford, UK, pp. 2-5.
- 1336 Rossi, S., 2003. Etude pollinique de la séquence lacustre Pléistocène de Piànico-Sèllere (Italie). Ph.D.  
1337 Thesis, Université de Droit d'Economie et des Sciences d'Aix Marseille III.
- 1338 Rouis-Zargouni, I., Turon, J.-L., Londeix, L., Essallami, L., Kallel, N., Sicre, M.-A., 2010. Environmental  
1339 and climatic changes in the central Mediterranean Sea (Siculo-Tunisian Strait) during the last 30 ka based  
1340 on dinoflagellate cyst and planktonic foraminifera assemblages. *Palaeogeogr. Palaeoclimatol. Palaeoecol.*  
1341 285, 17-29.
- 1342 Roussakis, G., Karageorgis, A.P., Conispoliatis, N. & Lykousis, V., 2004. Last glacial-Holocene sediment  
1343 sequences in N. Aegean basins: structure, accumulation rates and clay mineral distribution. *Geo-Mar.*  
1344 *Lett.* 24, 97-111.
- 1345 Ruddiman, W., Fuller, D., Kutzbach, J., Tzedakis, P., Kaplan, J., Ellis, E., Vavrus, S., Roberts, C., Fyfe, R.,  
1346 He, F., 2016. Late Holocene climate: Natural or anthropogenic? *Rev. Geophys.* 54(1), 93-118
- 1347 Saaroni, H., Bitan, A., Alpert, P., Ziv, B., 1996. Continental polar outbreaks into the Levant and Eastern  
1348 Mediterranean. *Inter. J. Climat.* 1996, 1175-1191.
- 1349 Saavedra-Pellitero, M., Flores, J.A., Baumann, K.-H., Sierro, F.J., 2010. Coccolith distribution patterns in  
1350 surface sediments of equatorial and southeastern Pacific Ocean. *Geobios* 43, 131-149.
- 1351 Sánchez Goñi, M. S., Cacho, I., Turon, J. L., Guiot, J., Sierro, F. J., Peyrouquet, J. P., Shackleton, N. J.,  
1352 2002. Synchronicity between marine and terrestrial responses to millennial scale climatic variability  
1353 during the last glacial period in the Mediterranean region. *Climate dynamics* 19(1), 95-105.
- 1354 Sánchez Goñi, M.F., Rodrigues, T., Hodell, D.A., Polanco-Martínez, J.M., Alonso-García, M., Hernández-  
1355 Almeida, I., Desprat, S., Ferretti, P., 2016. Tropically-driven climate shifts in southwestern Europe during  
1356 MIS 19, a low eccentricity interglacial: *Earth and Planetary Science Letters* 448, 81-93.
- 1357 Sangiorgi, F., Dinelli, E., Maffioli, P., Capotondi, L., Giunta, S., Morigi, C., Principato, M.S., Negri, A.,  
1358 Emeis, K.-C., Corselli, C., 2006. Geochemical and micropaleontological characterization of a  
1359 Mediterranean sapropel S5: a case study from core BAN89GC09 (south of Crete). *Palaeogeogr.*  
1360 *Palaeoclimatol. Palaeoecol.* 235, 192-207.
- 1361 Sauer, D., Wagner S., Brückner, H., Scarciglia, F., Mastronuzzi, G., 2010. Soil development on marine  
1362 terraces near Metaponto (Gulf of Taranto, Southern Italy). *Quat. Int.*, 222, 48-63.
- 1363 Savini, A., Corselli, C., 2010. High-resolution bathymetry and acoustic geophysical data from Santa Maria di  
1364 Leuca Cold Water Coral province (Northern Ionian Sea-Apulian continental slope). *Deep-Sea Res II* 57,  
1365 326-344
- 1366 Sbaffi, L., Wezel, F.C., Kallel, N., Paterne, M., Cacho, I., Ziveri, P., Shackleton, N., 2001. Response of the  
1367 pelagic environment to palaeoclimatic changes in the central Mediterranean Sea during the Late  
1368 Quaternary. *Mar. Geol.* 178, 39-62
- 1369 Siani, G., Paterne, M., Colin, C., 2010. Late glacial to Holocene planktic foraminifera bioevents and climatic  
1370 record in the South Adriatic Sea. *J. Quat. Sci.* 25, 808-821
- 1371 Siani, G., Magny, M., Paterne, M., Debret, M., Fontugne, M., 2013, Paleohydrology reconstruction and  
1372 Holocene climate variability in the South Adriatic Sea: *Climate Past* 9, 499-515, doi:10.5194/cp-9-499-  
1373 2013
- 1374 Sierro, F.J., Hodell, D.A., Curtis, J.H., Flores, J.A., Reguera, I., Colmenero-Hidalgo, E., Bárcena, M.A.,  
1375 Grimalt, J.O., Cacho, I., Frigola, J., Canals, M., 2005. Impact of iceberg melting on Mediterranean  
1376 thermohaline circulation during Heinrich events. *Paleoceanography* 20, PA2019.
- 1377 Simon, Q., Bourlès, L.D., Bassinot, F., Nomade, S., Marino, M., Ciaranfi, N., Girone, A., Maiorano, P.,  
1378 Thouveny, N., Choya, S., Dewil, F., Scao, V., Isguder, G., Blamart, D., and ASTER Team, 2017.  
1379 Authigenic  $^{10}\text{Be}/^{9}\text{Be}$  ratio signature of the Matuyama-Brunhes boundary in the Montalbano Jonico

1380 marine succession: Earth and Planetary Science Letters 460, 255-267,  
1381 <https://doi.org/10.1016/j.epsl.2016.11.052>.

1382 Simstich, J., Sarnthein, M., Erlenkeuser, H., 2003. Paired  $\delta^{18}\text{O}$  signals of *Neogloboquadrina pachyderma* (s)  
1383 and *Turborotalita quinqueloba* show thermal stratification structure in Nordic Seas. *Mar. Micropaleontol.*  
1384 48, 107–125.

1385 Socal, G., Boldrin, A., Bianchi, F., Civitarese, G., De Lazzari, A., Rabitti, S., Totti, C., Turchetto, M. M.,  
1386 1999. Nutrient, particulate matter and phytoplankton variability in the photic layer of the Otranto strait, J.  
1387 *Mar. Syst.* 20, 381-398.

1388 Spero, H.J., Williams, D.F., 1990. Evidence for seasonal low-salinity surface waters in the Gulf of Mexico  
1389 over the last 16,000 years. *Paleoceanography* 5, 963-975. <https://doi.org/10.1029/PA005i006p00963> .

1390 Spezzaferri, S., Kucera, M., Pearson, P.N., Wade, B.S., Rappo, S., Poole, C.R., Morard, R., Stalder, C.,  
1391 2015. Fossil and genetic evidence for the polyphyletic nature of the planktonic foraminifera  
1392 “*Globigerinoides*”, and description of the new genus *Trilobatus*. *PLoS One* 10 (5), e0128108.  
1393 <https://doi.org/10.1371/journal.pone.0128108>.

1394 Sprovieri, R., Di Stefano, E., Incarbona, A., Gargano, M.E., 2003. A high-resolution of the last deglaciation  
1395 in the Sicily Channel based on foraminiferal and calcareous nannofossil quantitative distribution.  
1396 *Palaeogeography, Palaeoclimatology, Palaeoecology* 202, 119-142.

1397 Sprovieri, M., Di Stefano, E., Incarbona, A., Manta, D. S., Pelosi, N., d'Alcalà, M. R., Sprovieri, R., 2012.  
1398 Centennial-to millennial-scale climate oscillations in the Central-Eastern Mediterranean Sea between  
1399 20,000 and 70,000 years ago: evidence from a high-resolution geochemical and micropaleontological  
1400 record. *Quaternary Science Reviews* 46, 126-135.

1401 Stein, R., Hefter, J., Grützner, J., Voelker, A., Naafs, B.D.A., 2009. Variability of surface water  
1402 characteristics and Heinrich-like events in the Pleistocene mid-latitude North Atlantic Ocean: Biomarker  
1403 and XRD records from IODP Site U1313 (MIS 16–9). *Paleoceanography* 24, PA2203.  
1404 <https://doi.org/10.1029/2008PA001639> .

1405 Stefanelli S., 2003. Benthic foraminiferal assemblages as tools for paleoenvironmental reconstruction of the  
1406 early-middle Pleistocene Montalbano Jonico composite section: *Bollettino della Società Paleontologica*  
1407 *Italiana* 42, 281-299.

1408 Stefanelli, S., 2004. Cyclic stages in oxygenation based on foraminiferal microhabitats: early-middle  
1409 Pleistocene, Lucania basin, southern Italy: *Journal of Micropaleontology* 23, 81-95.

1410 Stefanelli, S., Capotondi, L., Ciaranfi, N., 2005. Foraminiferal record and environmental changes during the  
1411 deposition of early-middle Pleistocene sapropels in southern Italy: *Palaeogeography, Palaeoclimatology,*  
1412 *Palaeoecology* 216, 27-52.

1413 Thunell, R.C., 1978. Distribution of recent planktonic foraminifera in surface sediments of the  
1414 Mediterranean Sea. *Mar. Micropaleontol.* 3, 147–173.

1415 Tolderlund, D.S., Bé, A.W.H., 1971. Seasonal distribution of planktonic foraminifera in the western North  
1416 Atlantic. *Micropaleontology* 17, 297-329.

1417 Triantaphyllou, M.V., Ziveri, P., Gogou, A., Marino, G., Lykousis, V., Boulobassi, Emeis, K.-C., Kouli, K.,  
1418 Dimiza, M., Rosell-Melé, A., Papanikolaou, M., Katsouras, G., Nunez, N., 2009. Late Glacial–Holocene  
1419 climate variability at the south-eastern margin of the Aegean Sea. *Mar. Geol.* 266, 182–197.

1420 Turchetto, M., Boldrin, A., Langone, L., Miserocchi, S., Tesi, T., Foglini, F., 2007. Particle transport in the  
1421 Bari canyon (southern Adriatic Sea). *Mar. Geol.* 246, 231-247.

1422 Trotta, S., Marino, M., Maiorano, P., Girone, A., 2019. Climate variability through MIS 20-MIS 19 in core  
1423 KC01B, Ionian Basin (central Mediterranean Sea). *Alpine and Mediterranean Quaternary* 32 (2), 2019, 1-  
1424 15, <https://doi.org/10.26382/AMQ.2019.10>.

1425 Tzedakis, P.C., Channell, J.E.T., Hodell, D.A., Kleiven, H.F., Skinner, L.C., 2012. Determining the natural  
1426 length of the current interglacial: *Nature Geoscience* 5, <http://dx.doi.org/10.1038/NCEO1358>.

1427 Ulbrich, U., Lionello, P., Belusic, D., Jacobeit, J., Knippertz, P., Kuglitsch, F.G., Ziv, B., 2012. Climate of  
1428 the Mediterranean: synoptic patterns, temperature, precipitation, winds, and their extremes. In: *The*  
1429 *Climate of the Mediterranean Region-From the Past to the Future*. Elsevier.

1430 Vetter, L., Spero, H.J., Eggins, S.M., Williams, C., Flower, B.P., 2017. Oxygen isotope geochemistry of  
1431 Laurentide ice-sheet meltwater across Termination I. *Quaternary Science Reviews* 178, 102-117.

1432 Vezzani, L., 1967. I depositi plio-pleistocenici del litorale ionico della Lucania. *Atti Acc. Gioenia Sc. Nat. in*  
1433 *Catania*, s. VI, 18: 159-180.



- 1434 Vincent, E., Berger, W.H., 1981. Planktonic foraminifera and their use in Paleoceanography. In: Emiliani, C.  
 1435 (Ed.), *The Oceanic Lithosphere The sea*, vol. 7. John Wiley & Sons, New York, pp. 1025-1119.
- 1436 Voelker, A.H.L., Rodrigues, T., Billups, K., Oppo, D., McManus, J., Stein, R., Hefter, J., Grimalt, J.O.,  
 1437 2010. Variations in mid-latitude North Atlantic surface water properties during the mid-Brunhes (MIS 9–  
 1438 14) and their implications for the thermohaline circulation. *Clim. Past* 6, 531-552.
- 1439 von Grafenstein, R., Zamm, R., Tiedemann, R., Murat, A., 1999. Planktonic  $\delta^{18}\text{O}$  records at Sites 976 and  
 1440 977, Alboran Sea: stratigraphy, forcing and paleoceanographic implications. In: Zahn, R., Comas, M.C. &  
 1441 Klaus, A. (Eds), *Proceedings of the Ocean Drilling Program, Scientific Results 161*, pp. 469-479.
- 1442 Wagner, B., Vogel, H., Francke, A. et al. 2019. Mediterranean winter rainfall in phase with African  
 1443 monsoons during the past 1.36 million years. *Nature* 573, 256–260. <https://doi.org/10.1038/s41586-019-1529-0>.
- 1444 Weaver, P.P.E., Pujol, C., 1988. History of the last deglaciation in the Alboran Sea (western Mediterranean)  
 1445 and adjacent North Atlantic as revealed by coccolith floras. *Paleogeogr. Paleoclim. Paleoecol.* 64, 35-42.
- 1446 Winter, A., Jordan, R.W., Roth, P.H., 1994. Biogeography of living coccolithophores in ocean waters. In:  
 1447 Siesser, W.G. (Ed.), *Coccolithophores*. Cambridge University Press, London, pp. 161-178.
- 1448 Wright, A.K., Flower, B.P., 2002. Surface and deep ocean circulation in subpolar North Atlantic during the  
 1449 mid-Pleistocene revolution. *Paleoceanography* 17, 1068. <http://dx.doi.org/10.1029/2002PA000782>.
- 1450 Xoplaki, E., Gonzalez-Rouco, J.F., Luterbacher, J., Wanner, H., 2003. Mediterranean summer air  
 1451 temperature variability and its connection to the large-scale atmospheric circulation and SSTs. *Clim. Dyn.*  
 1452 20 (7-8), 723-739.
- 1453 Ziveri, P., Baumann, K.-H., Boeckel, B., Bollmann, Young, J., Young, Y.R., 2004. Biogeography of selected  
 1454 Holocene coccoliths in the Atlantic Ocean. In: Thierstein, H.R. (Ed.), *Coccolithophores: From Molecular  
 1455 Processes to Global Impact*. Springer, Berlin, pp. 403-428.
- 1456 Zonneveld, K.A.F., Versteegh, G.J.M., Kodrans-Nsiah, M., 2008. Preservation and organic chemistry of Late  
 1457 Cenozoic organic-walled dinoflagellate cysts: a review. *Mar. Micropaleontol.* 86, 179-197.

1459  
 1460

1461 Figure captions

1462

1463 **Fig. 1. A:** location of the study area. **B:** Simplified regional geological setting of southern Italy. The  
 1464 location of the Montalbano Jonico section is indicated by the red star. Legend of the geological map  
 1465 in figure B: a) Cretaceous units of the Apulian Foreland; b) Calcareous units of the Plio-Pleistocene  
 1466 Apennines Foreland; c) Siliciclastic units of the Plio-Pleistocene Apennines Foreland; d) Lower  
 1467 Pleistocene regressive conglomerates of the Bradanic Trough; e) Middle-Upper Pleistocene marine  
 1468 terraced deposits of the Bradanic Trough; f) Triassic-Neogene units of the Apennines Chain; g)  
 1469 Quaternary volcanic units. **C:** lithological features of Montalbano Jonico composite section  
 1470 (Intervals A and B), with details on paleontological and oxygen isotope data at the Ideale section  
 1471 (Ciaranfi et al., 2010; Maiorano et al., 2010; Nomade et al., 2019). MD: maximum depth; MF:  
 1472 maximum flooding. The end of temporary disappearance of *Gephyrocapsa omega* is also shown on  
 1473 the Ideale section. **D:** main sea surface and subsurface water currents in the Ionian Sea, according to  
 1474 Gacic et al. (2010), redrawn (see text for details). MAW: modified Atlantic water; LIW/CIW:  
 1475 Levantine/Cretan intermediate waters; WAC: western Adriatic water.

1476

1477 **Fig. 2.** Quantitative abundance patterns of selected calcareous plankton taxa (F-O) and alkenone-  
 1478 SST (D), and benthic oxygen (C) and carbon (P) isotope records at the Ideale section. Modern  
 1479 annual SST (19.6°C) is shown on alkenone-SST record according to Pujol and Vergnaud-Grazzini  
 1480 (1995). A: mean summer insolation, obliquity and eccentricity (65° N) from Laskar et al. (2004). B:  
 1481 sea level curve; 19a1-19a3 are interstadial phases (yellow bars) during 19a according to Nomade et  
 1482 al. (2018). Stage boundaries and climate optimum are marked according to Nomade et al. (2019).  
 1483 Light blue bands on proxy records are stadial phases. Violet arrows indicate the main phases of  
 1484 ameliorated climate condition.

1485  
1486  
1487  
1488  
1489  
1490  
1491  
1492  
1493  
1494

**Fig. 3.** Quantitative abundance patterns of selected calcareous plankton taxa (D-G) and alkenone-SST (C), and benthic oxygen (B) and carbon (I) isotope records at the Ideale section. Star symbol in the sapropel interval is the acme occurrence of dinocyst *Polysphaeridium zoharyi* (Bertini et al., 2015; Maiorano et al., 2016a), that has been associated to Mediterranean sapropel formation (Giunta et al., 2006; Sangiorgi et al., 2006); diamond symbol in the sapropel interval is the increase episode of benthic foraminifera infauna/epifauna ratio (Stefanelli, 2003) as signal of stressed condition at the sea bottom (Marino et al., 2015). A: sea level curve. H: mean summer insolation (65° N) from Laskar et al. (2004).

1495  
1496  
1497  
1498  
1499  
1500  
1501  
1502

**Fig. 4.** Quantitative abundance patterns of selected taxa (E, G), pollen (F), benthic oxygen (B), alkenone-SST (C) and carbon (D) isotope records at the Ideale section. A: mean summer insolation (65° N) from Laskar et al. (2004); climate proxies from Iberian margin core U1385 (H-O), North Atlantic cores 980 (P-Q), 983 (R-S) are represented each in its original age model. Pink bands indicate intervals of climatic instability (see text). Light blue bands on proxy records are stadial phases. Stage boundaries and climate optimum/Tajo phase are marked according to Nomade et al. (2019) at the Ideale section, and according to Hodell et al. (2015) and Sánchez Goñi et al. (2016) at the Iberian margin.

Figure 1

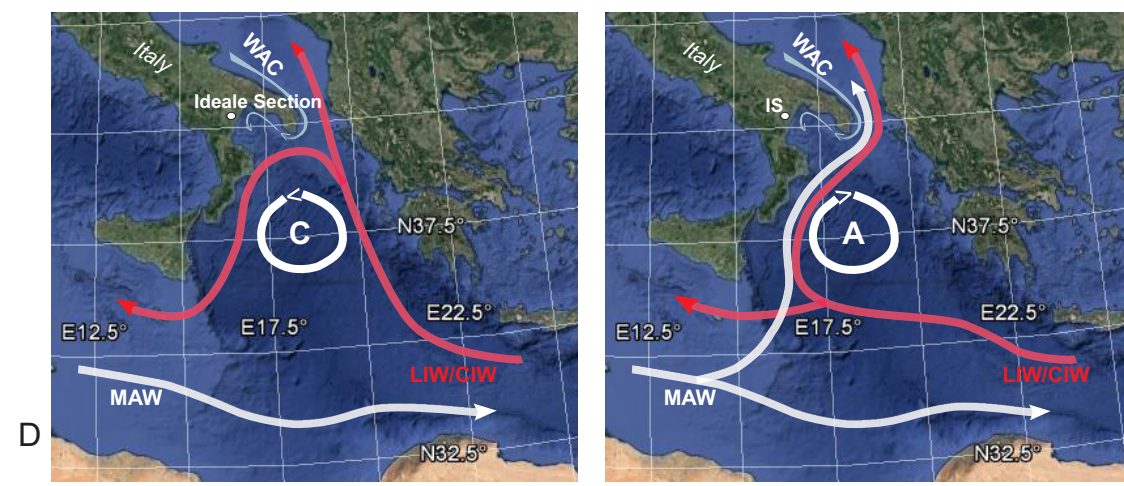
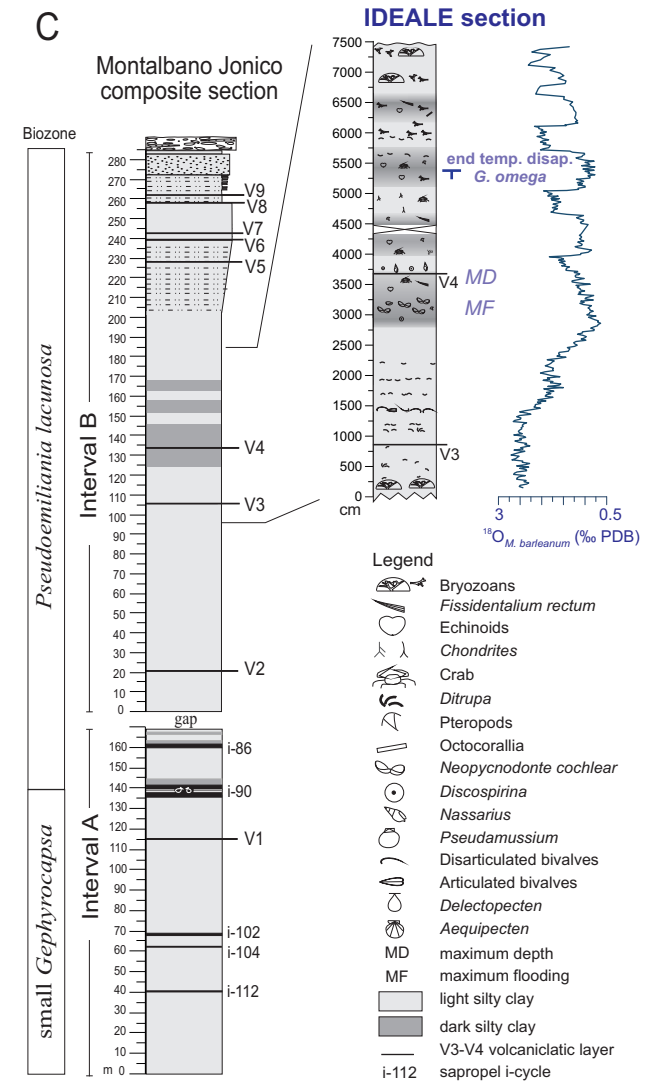
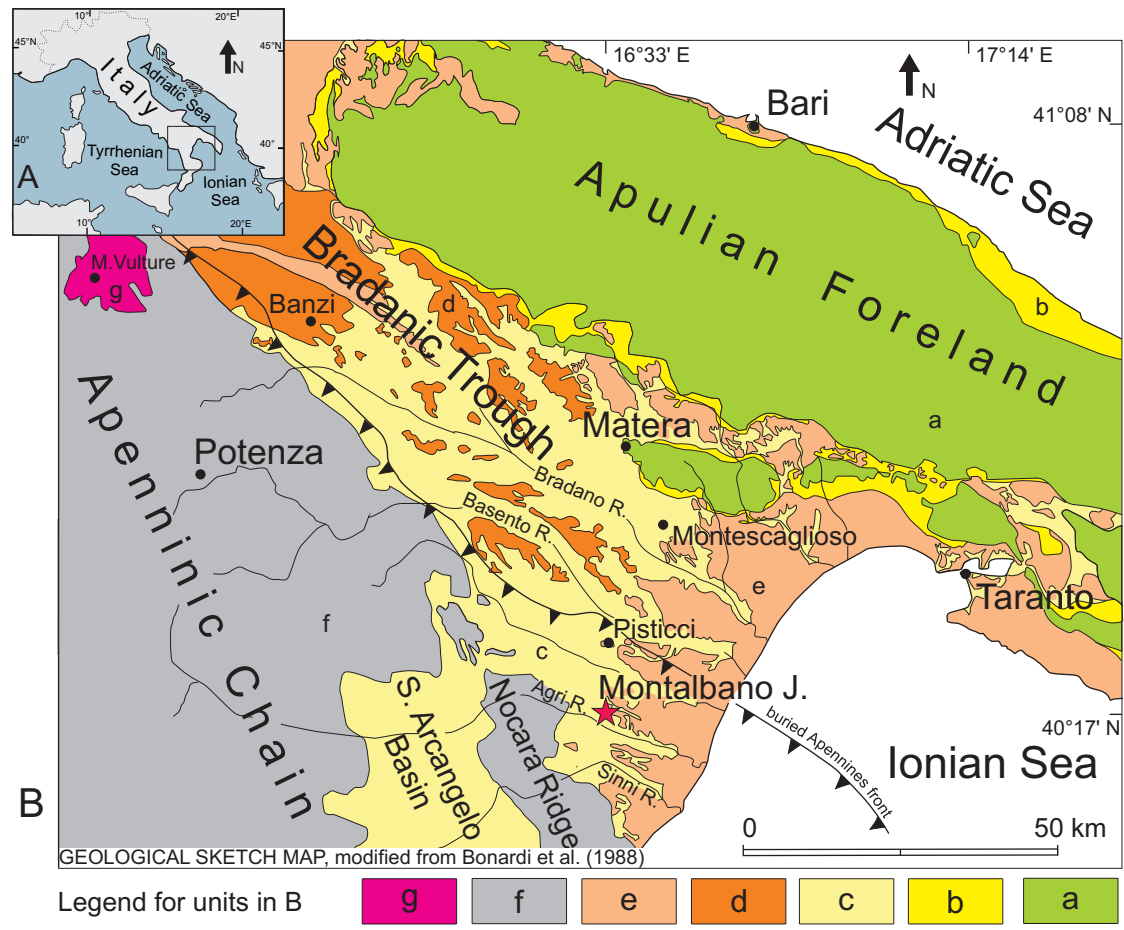


Fig. 1

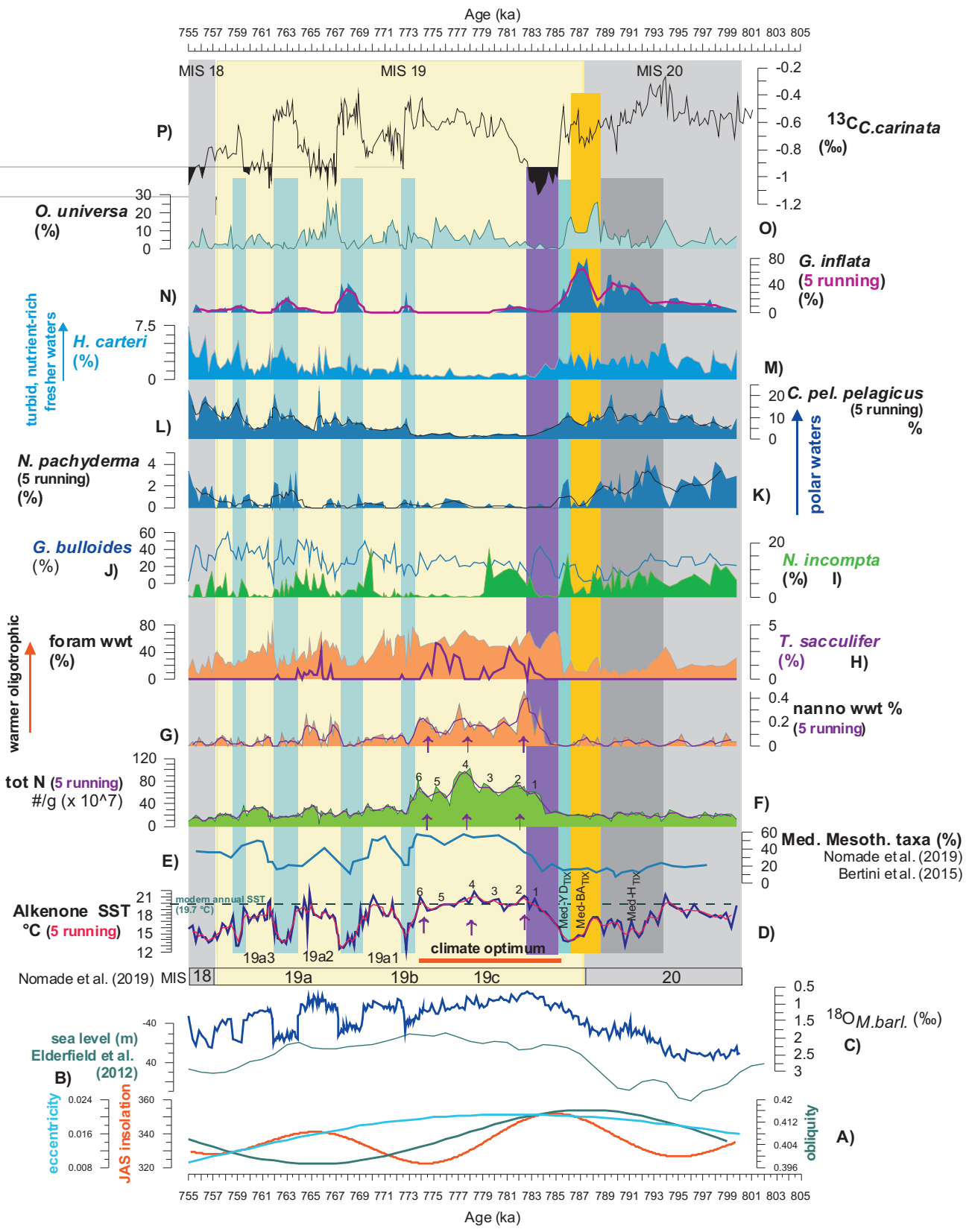


Fig. 2

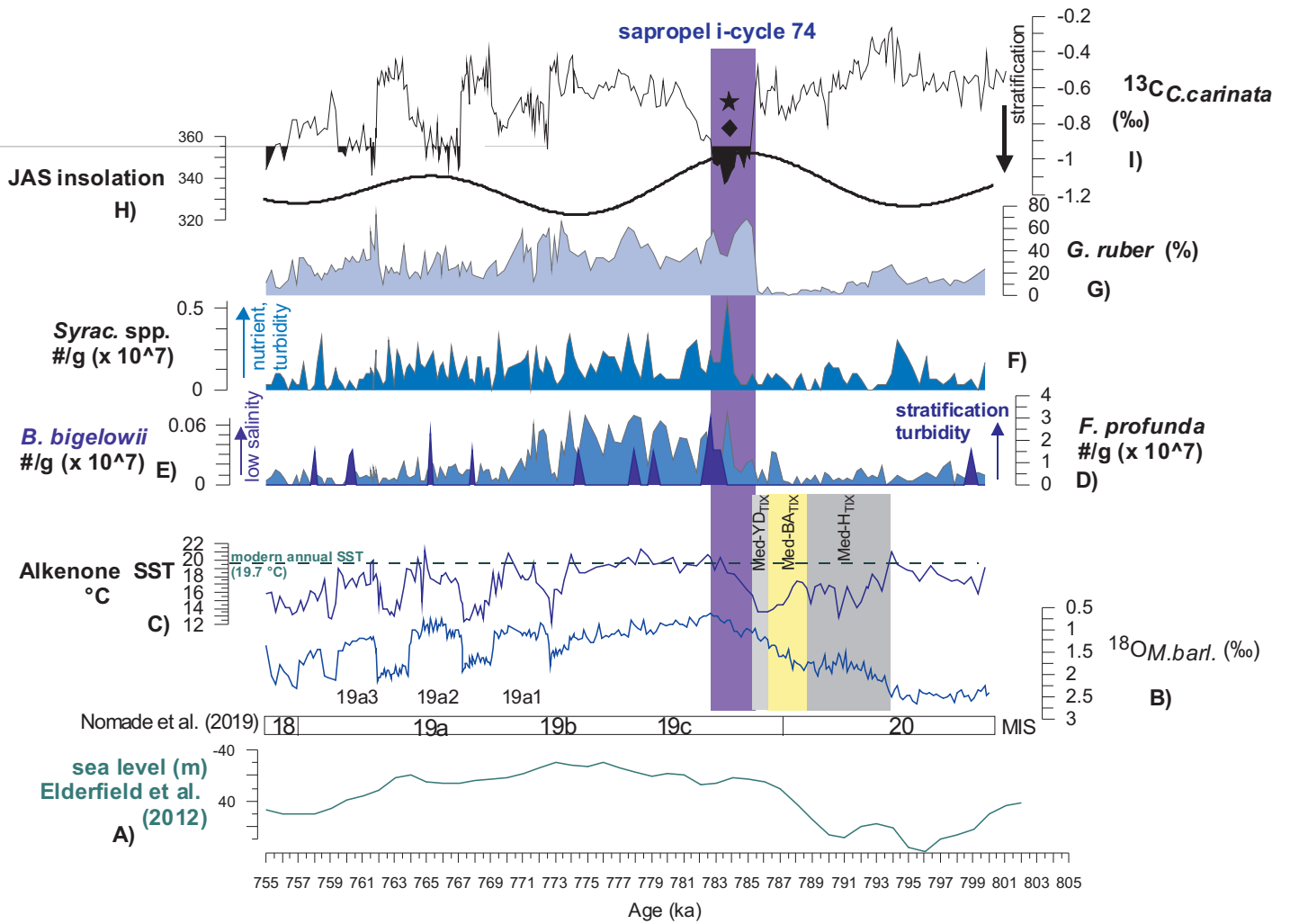


Fig. 3

Figure 4

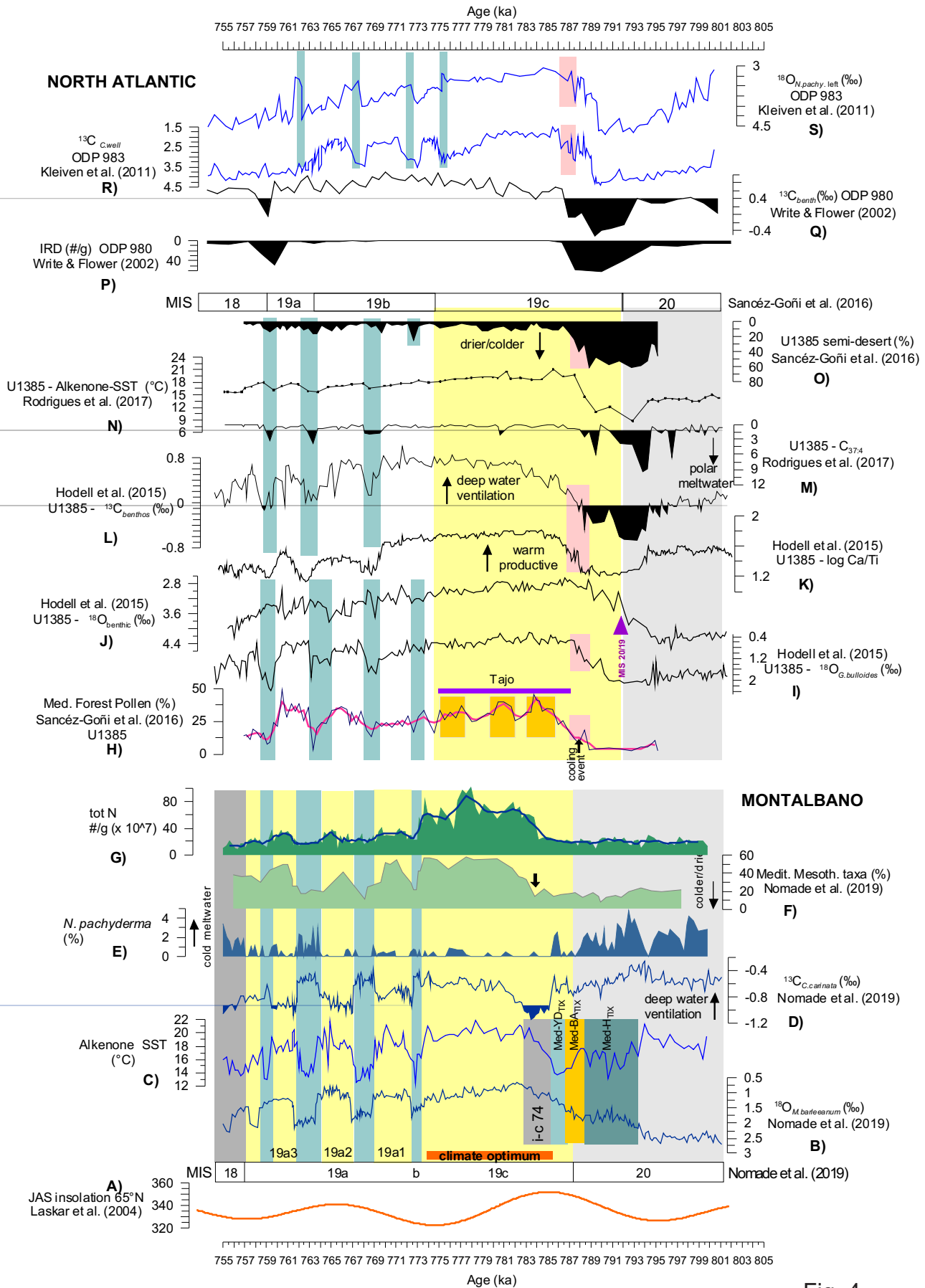


Fig. 4

**Declaration of interests**

The authors declare that they have no known competing financial interests or personal relationships that could have appeared to influence the work reported in this paper.

The authors declare the following financial interests/personal relationships which may be considered as potential competing interests:

Best Regards

*Mano Manis*



Click here to access/download  
**Supplementary Material**  
Marino et al. data.xls

